



Mälardalen University
School of Innovation Design and Engineering
Västerås, Sweden

Thesis for the Degree of Master of Science in Engineering - Robotics
30.0 credits (DVA502)

INTEGRATED LOCALIZATION AND DIRECTED COMMUNICATION FOR ACOUSTIC UNDERWATER SYSTEMS

Albin Barklund
abd11003@student.mdh.se

Daniel Adolfsson
dan11003@student.mdh.se

Examiner: Mikael Ekström
Mälardalen University, Västerås, Sweden

Supervisor: Martin Ekström
Mälardalen University, Västerås, Sweden

Company supervisor: Andrey Kruglyak,
Prevas AB, Västerås, Sweden

June 9, 2016

Abstract

During this master thesis a modem for integrated underwater acoustic localization and directed communication was developed. A transducer line array was designed and manufactured based on piezoelectric elements. The array was capable of beam forming to direct transmission and spatially filter received signals to apply a selective hearing towards the direction of other modems. Localization was implemented by estimating bearing and range for acoustic modems based on Time Difference of Arrival and Time of Arrival Respectively. A model was presented to relate Time Difference of Arrival to a bearing for a received acoustic wave. Extended Kalman Filter was used for filtering the position estimations. Communication using digital phase shift modulation was motivated and implemented. The modem was successfully tested in a pool environment where a high level of echo was measured. Echo was shown to have a significant impact in some of the cases. The work included PCB development, FPGA, transducer design and algorithms for localization and communication.

Table of Contents

1 Abreviations	5
2 Introduction	6
2.1 Background	6
2.1.1 Communication in the underwater channel	6
2.2 Related work	7
2.2.1 Underwater Acoustic Sensor Networks	7
2.2.2 Localization in UASN	7
2.2.3 Beamforming in underwater applications	7
2.3 Acoustic Communication Systems	8
2.4 Motivation	9
3 Hypothesis	10
4 Problem formulation	10
5 Expected outcome	11
6 Limitations	11
7 Method	12
7.1 Requirements	12
7.1.1 Hardware requirements	12
7.1.2 System requirements	12
7.1.3 Performance requirements	12
7.2 Testing	13
7.3 Planning	14
8 Transducer design	16
8.1 Beam pattern	16
8.1.1 Phase array	17
8.2 Power of the transducers	18
8.2.1 Source level	18
8.2.2 Transmission modeling	18
8.2.3 Acoustic noise	19
8.2.4 Hydrophone sensitivty	19
8.2.5 Passive sonar equation	19
8.2.6 Final design	20
8.2.7 Alternative transducer design	20
8.2.8 Piezo element pin mapping	21
9 Electronic design	22
9.1 NI USB-7845R	22
9.2 Motherboard	22
9.3 Power supply	23
9.4 Channel board	24
9.4.1 Piezo Driver	25
9.4.2 Relaxation of piezo elements	25
9.4.3 Amplifier filter and protection	25
9.5 Noise considerations	25
9.6 Test modem	26
9.6.1 MyRIO	26
9.6.2 Electronics design	26
9.7 Lessons learned	27

10 System design	29
10.1 Digital beamforming	30
10.1.1 Geometry analysis of beamforming	30
10.1.2 Beam forming in the digital domain	31
10.1.3 Resolution and sampling rate	31
10.1.4 Phase shift and sampling rate	32
10.1.5 Implementation on FPGA	33
10.2 Localization	33
10.2.1 Distance measurement	33
10.2.2 Angle of Attack	33
10.2.3 Localization algorithm	34
10.2.4 Synchronization	35
10.3 Communication	35
10.3.1 Binary differential phase-shift keying	35
10.3.2 Time Division Multiple Access	35
10.3.3 Transmitter	37
10.3.4 Receiver	37
11 Testing	39
11.1 Test rig	39
11.2 Phase controllability test, T1	41
11.3 Beamforming transmission test, T2	41
11.4 Beamforming reception test, T3	41
11.5 Communication test A, T4	41
11.6 Communication test B, T5	41
11.7 Angle of Attack test A, T6	41
11.8 Angle of Attack test B, T7	42
11.9 Localization test, T8	42
11.10 Planar wave propagation test, T9	42
12 Results	43
12.1 Phase controllability test, T1	43
12.2 Beam forming transmission test, T2	43
12.2.1 Test session 1	43
12.2.2 Test session 2	43
12.3 Beam forming reception test, T3	45
12.4 Communication test A, T4	45
12.5 Communication test B, T5	48
12.6 Angle of Attack test A, T6	49
12.7 Angle of Attack test B, T7	51
12.8 Localization test, T8	51
12.9 Planar wave propagation test, T9	52
12.10 Electronics and other results	53
12.10.1 PSU testing	53
12.10.2 Channel board testing	53
12.10.3 No load current	53
12.10.4 T/R switch	53
12.10.5 Channel board Input	54
12.10.6 Channel board input filter	55
12.10.7 Hardware in the loop RMS detector test	55
13 Requirements verification	56
13.1 System requirements verification	56
13.2 Hardware requirements verification	56
13.3 Performance requirements verification	56
14 Discussion	57

15 Conclusion	59
16 Future work	60
17 Acknowledgement	61
References	64

1 Abreviations

UAV	Unmanned Autonomous Vehicle
DSP	Digital Signal Processing
UAV	Unmanned Autonomous Vehicle
DSP	Digital Signal Processing
ISI	Intersymbol Interference
UASN	Underwater Acoustic Sensor Networks
GPS	Global Positioning System
ToA	Time of Arrival
TDoA	Time Difference of Arrival
USBL	Ultra Short Base Line
AoA	Angle of Attack
EKF	Extended Kalman Filter
SLAM	Simultaneous Localization and Mapping
DSSS	Direct-sequence spread spectrum
OFDM	Orthogonal frequency-division multiplexing
PSK	Phase-shift keying
FSK	Frequency-shift keying
TDMA	Time Division Multiple Access
SL	Source Level
RL	Receive Level
DI	Directivity Index
NL	Noise Level
DT	Detection Threshold Level
TL	Transmission Loss
SMA	SubMiniature version A connectors
PCB	Printed Circuit Board
FPGA	Field Programmable Gate Array
PSU	Power Supply Unit
ADC	Analog-to-digital converter
DIO	Digital Input Output
DAQ	Data Acquisition
MOSFET	Metal Oxide Semiconductor Field Effect Transistor
SoC	System on Chip
DMA	Direct Memory Access
DPSK	Differential Phase Shift Keying
FFT	Fast Fourier Transform
IFFT	Inverse Fast Fourier Transform
DRAM	Dynamic random-access memory
RMS	Root Mean Square
PC	Personal Computer

2 Introduction

The following work has been done as a master thesis at Malardalens University. The work is connected to the university's research in underwater robot systems and vision to create a swarm of collaborating robots[1].

2.1 Background

The demand for robust underwater communication is of increasing interest [2]. Application areas include remote control in oil industry, seafloor mapping, environmental systems, scientific exploration, video or audio transmission between divers and or Unmanned Autonomous Vehicles (UAV). Recent advancements in digital signal processing (DSP)[3] and computational hardware have led to significant progress in underwater acoustic communication increasing data throughput and transmission range [4]. Underwater communication is almost exclusively based on acoustic communication. Radio wave communication has been implemented but is limited to short distances because of rapid attenuation of radio signals in water. Optical methods provides good bandwidth and is very energy efficient, however they are limited in range due to scattering. The technique requires line of sight which causes problems in some applications. Optical communication capable of high data rates at relatively short distances has been implemented and is commercially available [4][5][6] [7] .

2.1.1 Communication in the underwater channel

The acoustic channel is recognized as one of the most difficult communication channels today, the technical issues are stated by J. Partan [6]. It poses several challenges that need to be considered. The propagation of acoustic waves in water should be modeled in order to establish a robust and reliable communication link. As with any other signal, acoustic waves attenuate with distance caused by spreading. In addition to distance the signal degradation is also dependent upon frequency; this is due to absorption, a conversion of acoustic energy into heat. Equation 1 describes the total path loss,

$$A(l, f) = \left(\frac{l}{l_r}\right)^k a(f)^{l-l_r} \quad (1)$$

where l is the transmission distance in relation to some reference l_r , f is the frequency band of the signal and k refers to the path loss exponent. This makes the acoustic channel very limited in bandwidth.

Sound waves propagates with a speed of approximately 1500 m/s in water, which is about $2 \cdot 10^5$ times slower than the propagation of radio waves. This causes high latency in the acoustic communication channel which needs to be considered when designing communication protocols. If neglected this can lead to an overall reduction in data throughput in an acoustic underwater network as described by J. G. Proakis [4]. The slow speed of sound can also cause signals transmitted or received by any mobile node to be distorted by the Doppler effect since the velocity of a moving node can be of significant proportion to the speed of sound. This can cause a shift in both frequency, phase and amplitude [6].

Multipath interference is another phenomenon caused by reflection of propagating waves. Signals will bounce from the surface and from the bottom of the ocean resulting in several propagation paths between transmitter and receiver. The signal will in other words arrive at different times and interfere with itself. Refractions will also alter the propagation path and cause multipath interference. Each of these propagation paths can be modeled accurately in still water conditions. But the presence of surface waves creates an time-variability in the channel [2]. This in terms creates a selectivity of different frequencies in the channel. This interference results in a phenomenon called fading where the signal partly or entirely cancels out and create spatial regions where no signal is present [6].

Multipath is usually the cause of Intersymbol Interference (ISI) and may require ISI compensation for the communication to function properly [2].

The term "time variation" encapsulates the changes in the propagation medium caused by environmental factors such as fluctuations in temperature, the absence or presence of waves, winds and currents.

2.2 Related work

This thesis integrates methods from different fields of research to evaluate the problem of integrating directed communication and localization. The related work is separated into corresponding research fields.

2.2.1 Underwater Acoustic Sensor Networks

Underwater Acoustic Sensor Networks (UASN) have been studied over the past decades. The technology enables deployment of nodes capable of monitoring the sea. The areas of usage include environmental and oceanographic studies, disaster prevention but also surveillance and military applications[8]. The nodes might be stationary or mobile. A stationary node can be fastened onto the seafloor or a floating buoy. Mobile nodes can be UAV's or floating freely. The difference has to be considered for the localization and the communication as the position of the sensor nodes may vary with time.

2.2.2 Localization in UASN

One of the important and challenging tasks in UASN's is localization that is a requirement for robot swarms to perform a collaborative tasks. Localization is also needed for stamping acquired data with location of measurement. Underwater localization has been challenging due to the fact that conventional approaches such as Global Positioning System (GPS) cannot be deployed on underwater nodes. Localization has been done for UASN using multilateration on distance measurements between the unknown node and nodes at known positions. The distance is obtained using Time of Arrival (ToA) for synchronized or unsynchronized systems. This is feasible as acoustic waves propagates slowly under water which makes it possible to measure the ToA with high accuracy using inexpensive hardware. A second approach to localization is using the angle between nodes, the angle can be obtained measuring the Time Difference of Arrival (TDoA) using a sensor array[9]. The techniques generally assumes a far field transmission source. The angle is generally referred to as Angle of Attack (AoA).The sensor array of closely displaced sensors is referred to as Ultra Short Baseline (USBL) technology. A third approach combines the angle between the nodes with distance to obtain a better position estimation. The mentioned approaches are all used extensively in UASN as ToA or AoA measurements can be obtained from the acoustic modem already integrated into the sensor nodes.

The area of localization can be categorized into centralized and decentralized methods. In centralized localization methods, one node is assigned to calculate the position of the other nodes. Whereas in distributed methods all nodes take part of the localization process.

Localization algorithms can be further divided into estimation- or prediction-based algorithms. Estimation solves the problem of calculating the position based on distance readings or other current information. Prediction-based localization solves the problem of estimating the state of a node given the previously predicted position and position measurement. Prediction localization methods are of huge importance for both underwater and terrestrial localization. Extended Kalman Filter (EKF) and particle filter-based prediction algorithms have successfully been deployed to UAV's. They perform sensor fusion to combine position measurement with velocity measurement[10], these provide a basis for high accuracy and robust localization as they can handle the absence of position measurements by relying on the odometry. The application for the algorithms is Simultaneous Localization and Mapping (SLAM), the algorithm attempts to map static landmarks in the environment and use them to localize the moving robot[11].

2.2.3 Beamforming in underwater applications

Beamforming is a spatial filtering and transmission technique which can be adopted using an array of antennas. When combining the array with signal processing, the direction of transmission and reception as well as the beam pattern can be adjusted [12]. This is realized by controlling the phase

and amplitude for the individual array elements. Beamforming can be static or adaptive, static beamforming can be used if the conditions are not changed during transmissions such as having nonmoving transducers. Adaptive beamforming on the other hand, can change the direction of transmission and reception on the fly.

There are a set of algorithms for adaptive beamforming including “Minimum Mean-Square Error”, “Maximum Signal-to-Interference Ratio”, “Minimum Variance”. They can be used when information on the expected signal waveform, strength of the desired signal, signal shape and direction, respectively is available[13]. Practically, the methods are based on finding the complex weight vector which minimizes the difference between actual signal and expected signal. The problem of finding the weight vector to minimize the error is solved recursively using gradient descent[14]. Beamforming has also been used for sonar applications for decades and also as a spatial filter for receiving acoustic communication[15], however, little work has been done on analysis of communication by directed transmission.

2.3 Acoustic Communication Systems

The following manufacturers have underwater acoustic modems available on the market.

EvoLogics [16] state they have the most advanced and reliable systems. One of their product series of modems for position and communication is named “S2CR”. Positioning is based on USBL.

DSPComm [17] sells the modem “AquaComm” which are using Direct-sequence spread spectrum (DSSS) or Orthogonal frequency-division multiplexing (OFDM) for modulation.

TRITech [18] with their modem “MicronModem” which uses DSSS for modulation.

Woods Hole Oceanographic Institution [19] have developed the “Micromodem” which uses Phase-shift keying(PSK) or Frequency-shift keying(FSK.)

TeledyneBenthos [20] have developed the modem Benthos DAT which uses PSK and Multiple Frequency modulation (MFSK) and USBL for positioning.

LinkQuest [21] have developed a series of omnidirectional and directional long range modems for transmission up to 10km. The product “UWM2000H” can communicate in shallow water environment with harsh multipath conditions.

There are also some research groups working with underwater acoustic modems. The Information Sciences Institute at University of Southern California, are working with high latency and underwater sensor networks. They have been working with hardware for a low cost modem underwater acoustic modem but have not preceded to underwater testing[22].

University of California, Santa Barbara proposed a modem “AquaNodes” 2005. Two year later, they published their work of a functional modem based on a hybrid transducer. The modem uses acoustics for long range transmission and includes localization functionality based on USBL. For short range transmission within line of sight, optical technology is used [23]. The medium access and synchronization is based on Time Division Multiple Access (TDMA).

Researchers at School of Electrical and Electronic Engineering Newcastle University Newcastle proposed a modem called “Seatrac” which is using USBL for position estimation and DSSS modulation for communication at a data rate of 100bps [24]. Milica Stojanovic developed a reconfigurable hardware platform for rapid development and testing of methods for underwater communication and building UASNs. The modem was designed for development and simulation in Simulink [25].

2.4 Motivation

To the best of our knowledge, there's no approach of an integrated communication and localization system which explicitly models positions and uncertainties of nodes and uses this information for beamformed transmission. We are of the belief that this approach can be a good basis to obtain a robust communication and solve robotics tasks, ultimately within a mobile multi-node UASN.

3 Hypothesis

Adaptive beamforming can be extended from handling static to mobile nodes in an ultrasonic based acoustic point to point network by utilizing localization techniques. By doing this, the robustness in communication will be increased by preventing degradation in the direction of beam forming.

4 Problem formulation

In order to implement a system for testing the hypothesis, the following problems and tasks have been identified.

1. Make specifications and then develop or find a hardware platform that can solve the problems of adaptive beamforming, communication and localization based on ultrasonic transducer technology.
2. Find suitable communication protocols and modulation techniques in terms of implementation complexity and data rates, focusing on the physical and data link layer.
3. How can localization functionality be integrated in the communication system in an efficient way while keeping the overhead of navigation data transfer down?
4. How can the localization be modeled and implemented. What is required to continuously track nodes?
5. How can the adaptive beam forming be integrated with a localization system to direct the beam forming towards the receiving node?

5 Expected outcome

The desired outcome is to demonstrate that it is possible to integrate directed communication and localization within an acoustic modem to achieve a robust communication in mobile underwater sensor node applications. As the mobile node uses a conventional approach to robotics localization and data fusion, the localization algorithms could be extended with more sensors to provide a better communication link. Adaptive beam forming and directed transmission has been little used within underwater communication systems, hopefully the functionality will be proven useful. The prototype developed within this system will be a base for further underwater communication system research at Mälardalens University, ultimately it is desired to develop a modem for usage within swarms.

6 Limitations

Localization and beamforming will be implemented on 2D instead of 3D. The limitation is necessary to focus the work towards answering the hypothesis. The project will focus on creating a platform capable of performing integrated localization and communication between 2 nodes only. Problems arising when more nodes appear in the environment are not considered.

The distance between the modems is limited to 25m. The size, energy consumption and transmission strength is not considered. The nodes are synchronized before the experiments are performed by cable. There are methods for synchronization based on a 2 way travel time which are sufficient to measure the distance between nodes.

7 Method

During this master thesis the majority of the work was done following an iterative and quantitative engineering methodology; however, testing has to an extant also been qualitative. Development have been done following a top to bottom approach where the complete system have been broken down into smaller pieces. Verification and testing has been done following a bottom to top approach.

7.1 Requirements

The problem formulation was divided into a set of requirements.

7.1.1 Hardware requirements

- H1:** The hardware shall be able to handle directional transmission and reception using phase array based on piezoelectric elements.
- H2:** The hardware shall be able to estimate angle of attack of received signals.
- H3:** The frequency and gain of the transmitted signal shall be controllable.
- H4:** Phase of the individual piezo elements shall be controllable.
- H5:** The received signal gain and filter shall be controlled by software.

7.1.2 System requirements

- S1:** The system shall be able to perform simultaneous localization and directed communication with one other node.

7.1.3 Performance requirements

- P1:** Maximum steering angle ± 30 degrees.
- P2:** The system shall allow for directed communication with an effective data rate at 0.4 kbit/s over a range of 20 meter.
- P3:** The system shall predict the bearing angle to a sender node with 5 deg accuracy of estimation for a static node.
- P4:** The system shall estimate the distance to a sender node with an longitudinal error of 3 meters.

7.2 Testing

In order to verify that the requirements for the integrated communication and localization modem are met a set of tests have been designed. Each test are marked with the requirement they confirm. The tests are described in detail in section 11.

T1, Phase controllability test: This test verifies requirements **H3** and **H4**.

T2, Beamforming transmission test: This test verifies that beam former is capable of transmitting directional signals. Together with the Beam forming reception test this test verifies requirement **H1** and **P1**.

T3, Beamforming reception test: This test verifies that the beam former is capable of receiving directional signals. The test partially verifies requirement **H1** and **P1**.

T4, Communication test A: This test verifies non directional short range communication and partially verifies **P2**. The test verifies **H5**.

T5, Communication test B: This test verifies non directional short range communication and partially verifies **P2**. The test verifies **H5**.

T6, Angle of Attack test A: This test verifies the modem is capable of estimating angle of attack. This test verifies requirements **H2** and **P3**.

T7, Angle of Attack test B: This test verifies the modem is capable of estimating angle of attack. This test verifies requirements **H2** and **P3**.

T8, Localization test: This test verifies the modem is capable of estimating the distance between nodes. This test verifies requirement **P4** and partly verifies **S1**.

T9, Planar wave test: This test evaluates the degree of which the assumption of planar wave propagation applies and should verify the modeling.

7.3 Planning

The following tasks are planned for the thesis. The goal of the task "System design 1" is to make a diagram describing the different subsystems and asses if problems are solved using soft-or hardware.

The hardware of the planning is divided into sonar specifications and electronics development. The transducer with the specifications derived in Task Id 4 is manufactured together with "DeepVision", a company in Linkoping specialized in the area of piezoelectric vision sensors.

The electronics development process flow for one iteration is shown in Task Id 5-9. The electronics system is developed in modules, functionality and performance test are done for the separate modules as well as for integrated system shown in Task Id 9.

After hardware is completed, the tasks of angle of attack and beamforming are performed. The testing of the tasks will verify the hardware specifications as they are tasks assumed to be most sensitive of design errors. The last part of the development includes time of arrival estimation, communication and localization.

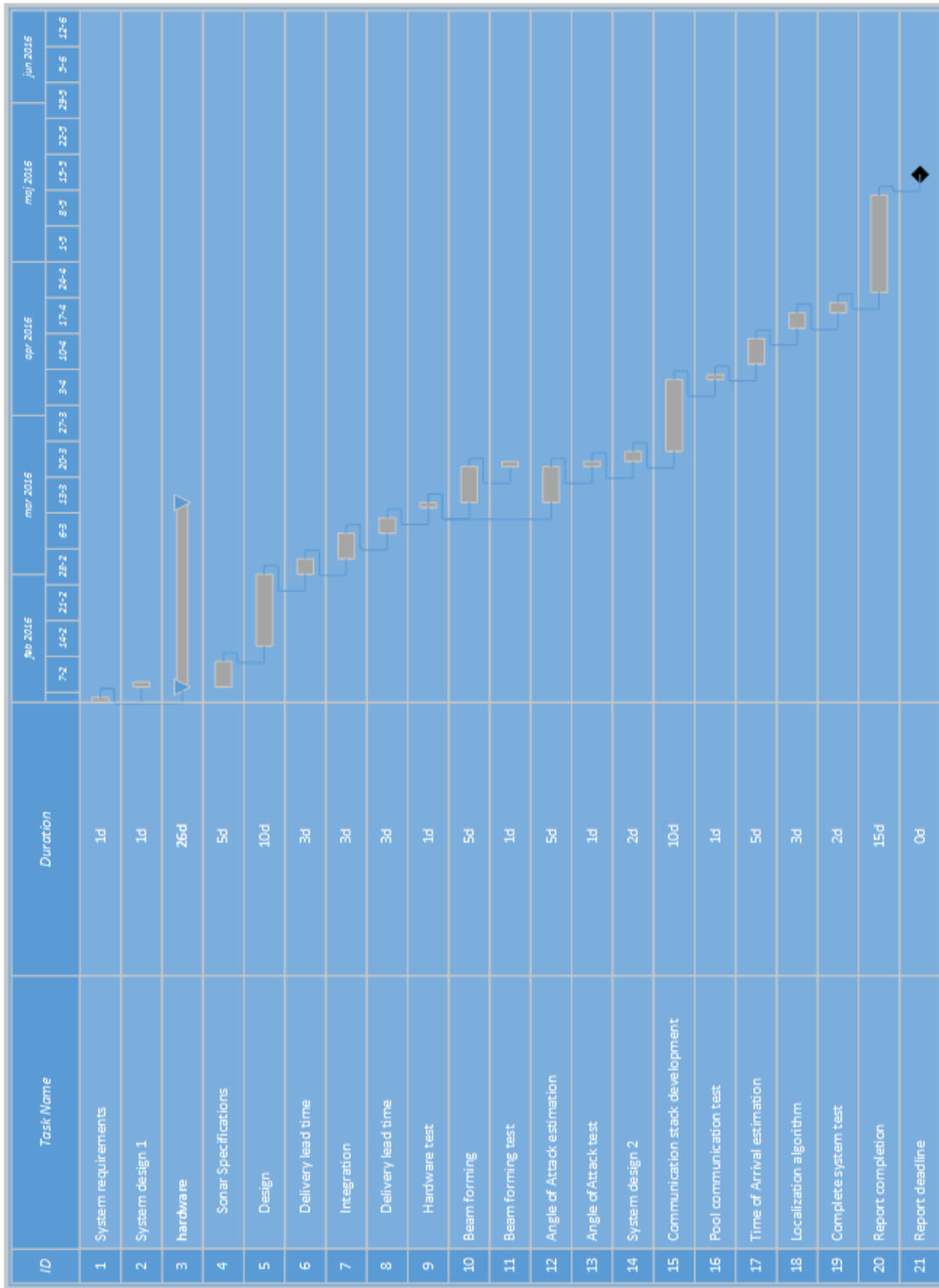


Figure 1: The the time plan of the master thesis, starting with system design and hardware development flowed by software development, testing and verification. The report was written in parallel with the other tasks during the whole project.

8 Transducer design

A transducer allow for conversion between acoustic and electric energy in both transmission and reception. Piezo-electrical elements were chosen for the transducers, they are inexpensive and can easily be manufactured in different sizes and shapes which determines the electronic and mechanical properties of the elements. In this application, the most important properties are directivity pattern, efficiency and resonance frequency. The voltage response is the relation between applied voltage over the element and the generated acoustic energy. The efficiency of the transducer is defined as the ratio between applied electronic and generated acoustic energy. The directivity of an element provides a measure of the radiated beam pattern. If placing the elements nearby each other, the individual beam patterns produce an interference pattern such that some directions experience constructive interference while other directions experience destructive interference. These phenomenon are caused by the principle of superposition. Depending on phase array parameters, the radiation pattern may have one or more lobes. The lobe caused by the highest constructive interference is called the main lobe, the direction of the lobe is referred to as the Maximum Response Axis (MRA). If the side lobes are greater than the main lobe they are referred to as grating lobes. Other directions of constructive interference are called sidelobes. Nulls are the directions where the waves produce a negative interference. This constellation is generally referred to as phase array, by varying the phase of the array elements the direction of the main lobe can be steered[26].

All design and measurements are done with respect for the Far-field of the transducer. The far-field is the distance from the transducer to where the models for spherical spreading and superposition apply. In the near field, the amplitude and phase of receiving signal are unpredictable due to the length of the transducer not being negligible compared to the transmission distance. Equation 2 defines the distance to the far field,

$$d \geq \frac{L^2}{2\lambda} \quad (2)$$

where L is the transducer length[26]. A 6 elements transducer with a spacing of $\lambda/2$, operating at a frequency of $40kHz$ has a Length of 9,25 cm. The corresponding far field is hence $\approx 12cm$.

8.1 Beam pattern

The following section attempts to propose the geometrical formation of the elements required for beamforming and angle of attack estimation according to the hardware requirements. The task is to steer the main lobe in the plane parallel to the pool, however it is not desired to send acoustic energy towards the bottom or the surface which will cause undesired multipath arrivals at the receiver. In order to have significantly different vertical and horizontal beam pattern, a rectangular based element was chosen. The beam pattern of a single transducer depends on the width w and height h as shown in figure 4. Equation 3 provides an estimation for the radiation pattern of a single element transducer

$$b(\theta) = \frac{\sin \frac{\pi L}{\lambda} \sin \theta}{\frac{\pi L}{\lambda} \sin \theta} \quad (3)$$

where L is the length of the side producing the beam pattern. It is based on the assumption that the vertical and horizontal beam patterns are independent. The formula i hence used to estimate the vertical and horizontal beam pattern separately. Using the formula we can estimate radiation patterns of individual elements, the vertical and horizontal patterns are shown in figure 2 and 3. Using a height of $h = 40mm$, the vertical pattern is quite narrow. This allows for directed fixed transmission among the pool plane. The horizontal beam pattern of an element is nearly omnidirectional at a width of $w = 4mm$ which is required in a phase array to maintain strength of the main lobe while steering the beam.

The directivity index is a measure of the spreading of beam pattern and is defined by equation 4

$$D_I = 10 \cdot \log \frac{I_0(r)}{(4\pi r^2)} \quad (db) \quad (4)$$

at a distance r from the source. In other words, 4 defines the ratio between the intensity produced in the direction of the main lobe and intensity produced by an omnidirectional transducer expressed in db . Due to the proposed width w , the directivity of the horizontal pattern is close to 0 as the pattern is close to begin omnidirectional[27].

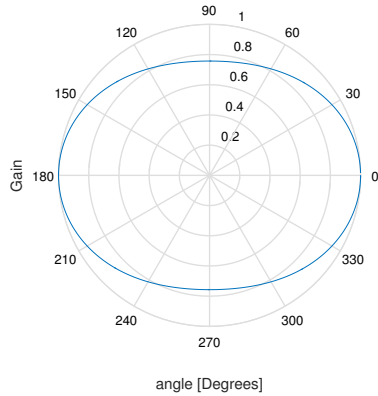


Figure 2: Horizontal beam pattern of a single transducer due to a width w of the rectangular piezoelectric elements. It is considered omnidirectional

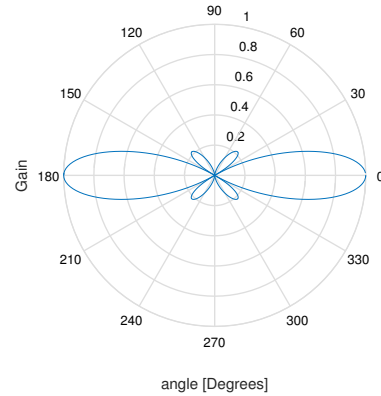


Figure 3: Vertical beam pattern of a single transducer due to a height h of the rectangular piezoelectric elements. It is considered to have a high directivity

8.1.1 Phase array

The elements were placed in a line array as shown in figure 4, this allows for steering the beam in the desired plane. The characteristics of the main lobe depends on the individual elements, their operating frequency and spacing distance. Assuming that the horizontal beam pattern is omnidirectional, the transducer array gain in the acoustic axis depends on the number of elements used. More elements produce a higher directivity index for the phase array transducer. Figure 5 illustrates how the horizontal beam pattern varies with the number of elements in the phase array.

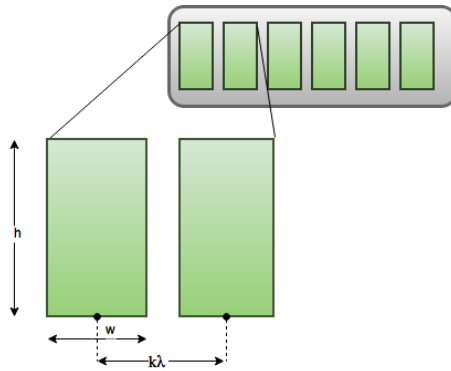


Figure 4: Geometry of the individual elements and the complete transducer array. The array consists of 6 elements with dimensions $width \times height \times thickness$, distanced by a scalar k of λ . The elements vibrate in the direction of the thickness, perpendicular to the width and height plane.

The elements in the figure 4 are placed with a spacing $k\lambda = \frac{1}{2}\lambda$. Six elements was chosen as it produces a distinct array gain, described in figure 5, while the complexity of electronics manufacturing is kept to a feasible level. When $k \leq \frac{\lambda}{2}$, the directivity index for a linear array can be approximated by equation 5 [26].

$$DI = 10 \log n = 10 \log 6 = 7.78 \quad (db) \quad (5)$$

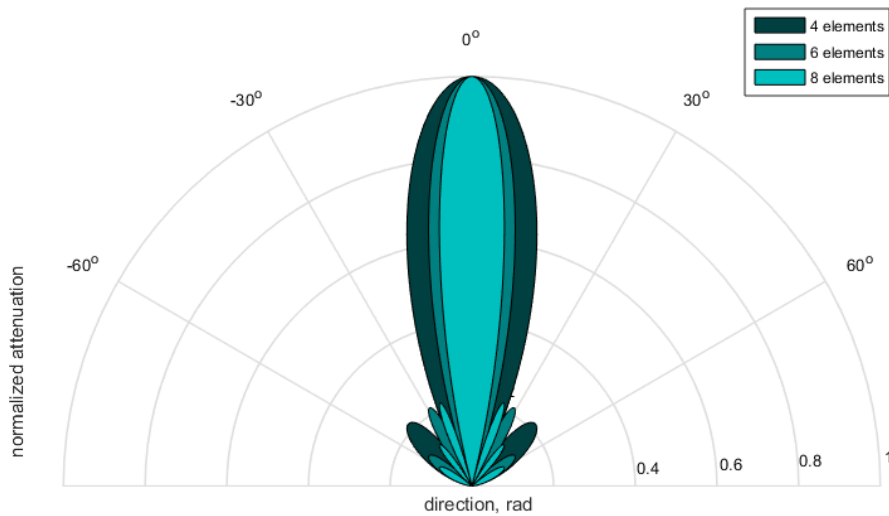


Figure 5: Horizontal beam pattern generated by a four, six and eight piezo elements array respectively. Six elements was chosen for the final design since it provides sufficient signal strength and keeping the complexity of electronics to a feasible level.

8.2 Power of the transducers

The following section investigate the electrical effect required to send ultrasonic based acoustic communication over a distance of 25 m. Conversion from electrical energy to acoustic energy are discussed in order to model spreading and absorption losses. Additionally, the impact of transducer specific parameters such as transmitting and receiving intensity are included in the section.

8.2.1 Source level

The source level describes the intensity of a propagating wave in the far field that a source can produce in the the direction of the main lobe. Equation 6 describes how the the source level is defined,

$$SL = 10 \cdot \log \frac{I_{source}}{I_{ref}} \quad (6)$$

where I_{ref} is a reference intensity defined as $1\mu P_a$ at $1m$. Equation 7 describes the source level intensity for a transducer,

$$SL = 10 \cdot \log P + DI + 170,9 + 10 \cdot \log E \quad (db) \quad (7)$$

where P is the transmitted electrical power, DI is the transducer directivity index of the transducer, the directivity causes a gain in the MRA which increase the source level. 170.9 is a factor for converting effect into source level and E is the factor of efficiency of conversion[26, 28].

8.2.2 Transmission modeling

Transmission loss is measure of the intensity loss due to absorption and spreading of the transmitted wave. The Transmission loss is defined as the difference between the source level and receiver level intensity $TL = 10 \log \frac{I(1_s)}{I(r)}$ assuming transmission in the MRI. Absorption is related to the the transmission distance, frequency and medium properties. Absorption loss can be estimated by equation 8,

$$TL = \alpha \cdot r \cdot 10^{-3} \quad (db) \quad (8)$$

where α is the absorption constant and r is the distance in km . In the book “Sonar for engineers”, table 3.1 [27], alpha is estimated to 17 at $50kHz$ at 15 degree celsius in sea water. The corresponding absorption loss is $TL = 17 \cdot 25 \cdot 10^{-3}$.

Intensity will lower due to spreading as the energy of the wave is expanded over a volume which increase with distance. Spreading loss depends on the geometrical form of the spreading and is given by $PL = 10 \cdot \log r$ and $PL = 20 \cdot \log r$ for cylindrical and spherical spreading respectively [27]. The pessimistic model of spherical spreading was chosen to account for other non-modeled losses. Assuming a transmission loss TL according to equation 10, the intensity at the receiver is defined by equation 9.

$$RL = SL - TL \quad (9)$$

$$TL = 20 \log r + \alpha \cdot r \cdot 10^{-3} = 20 \cdot \log r + 17 \cdot r \cdot 10^{-3} = 29 \quad (db) \quad (10)$$

8.2.3 Acoustic noise

There are lots of background noise included in the signal received by the hydrophone. Some of these sources are thermal noise, ambient noise and self generated noise. Thermal noise is generated from heat over resistive components and can hence be found in the transducer. The noise is given by the formula $V_{rms} = \sqrt{4K_b T R}$ per bandwidth where k_b is the boltzmann’s constant, T is the temperature of the component and R is the Resistance of the component.

Ambient noise can come from waves, ships, animals and humans. Self generated noise can be an echo of acoustic wave transmitted by the hydrophone. The magnitude of the noise depends on the environment in which the hydrophone operates.

8.2.4 Hydrophone sensitivity

The hydrophone sensitivity describes the transducer’s ability to convert a pressure p to a voltage v and is defined by equation 11.

$$\begin{aligned} S_h &= 20 \log \frac{p}{V} = 20 \log p - 20 \log V \Rightarrow \\ 20 \log V &= 20 \log p - S_h \Rightarrow \\ V &= 10^{\frac{20 \log p - S_h}{20}} \end{aligned} \quad (11)$$

8.2.5 Passive sonar equation

Equation 12 is called the passive sonar equation and describes the relation between signal, noise and detection threshold,

$$RL - N > DT \quad (dB) \quad (12)$$

where RL is the interesting signal level at the receiver, N is the noise level and DT is the detection threshold. The equation states that the SN signal is equal to the detection threshold. Knowing that S has propagated from the source location to the target location it can be expressed as the difference between the two, $S = SL - TL$, inserting the expression into equation 12 yeilds equation 13.

$$(SL - TL) - N > DT \quad (dB) \quad (13)$$

8.2.6 Final design

The thickness is chosen so that the resonance frequency is set to 40kHz. The following specifications were chosen for the modem.

1. Linear array of 6 elements
2. Element $w \times h \times t = 4 \times 40 \times t$ (mm)
3. Spacing of $k\lambda = 0.5\lambda$
4. Transmission loss of 29 (dB)
5. Received voltage $> 100mV$
6. 20m transmission length

In the specifications, the hydrophone sensitivity and efficiency parameters are missing. These properties are specific for piezo element and mechanical encapsulation. The parameters were not specified from DeepVision, however they can be estimated using an acoustic measurement probe with known sensitivity.

8.2.7 Alternative transducer design

Due to long production time of the transducer, there was not time to integrate the design within the scope of the master thesis. Instead an alternative solution was used based on off-the-shelf encapsulated piezoelectric ultrasonic transducers by Ekhult [29].

The beam pattern of the piezo elements is depicted in figure 6. Omnidirectional beam pattern

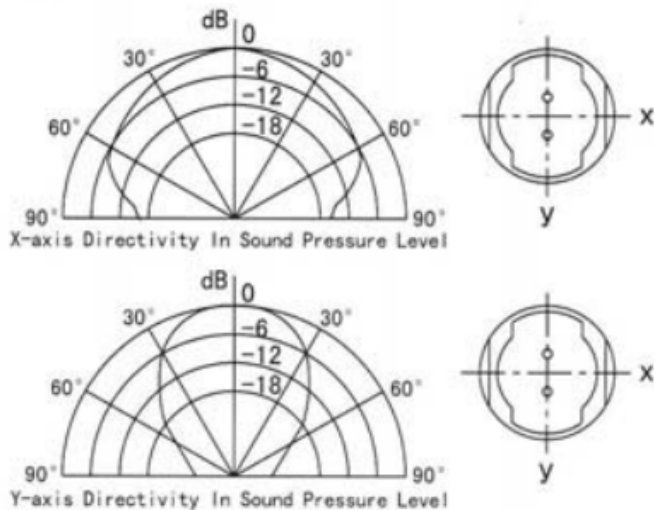


Figure 6: Horizontal and vertical beam pattern of the piezo elements used in the alternative design.¹. The wide horizontal beam pattern enables the beamformer to direct the beam while the narrow vertical beam pattern prevent unnecessary vertical spreading.

was assumed for the horizontal axis. The vertical beam pattern reaches a 3db attenuation at $\pm 30^\circ$. The elements have a resonance frequency of 40kHz. The transducer array was manufactured by soldering the piezo elements and SubMiniature version A connectors (SMA) onto a Printed Circuit Board (PCB). Silicon was used to electronically isolate the transducers. The chosen piezo element are not polarized, however one of the pins on the element was electrically connected to the transducer casing. The case pin was connected to the ground in the electronics and left electrically exposed to the water. All other conductive parts on the transducer was insulated by silicone and all excessive

¹Picture taken from the datasheet of A-14P20 [29].

PCB copper was removed. Conductivity test was performed before all tests. Figure 7 shows the manufactured transducer array.



Figure 7: The manufactured transducer array based on the alternative piezo elements from Ekhult. Six elements was used in the design. The board was manufactured at Mälardalen University.

8.2.8 Piezo element pin mapping

The electrical model of a piezo element does not have a polarity, however the electrical to mechanical properties have a polarity which causes a high or low voltage to mechanically expand or collapse the element respectively. During the testing, the polarity of the chosen piezo element does not correspond to the long and the short pin attached to the casing respectively. The error may not be of importance in general ultrasonic sensor applications, however the task of beamforming require high resolution phase control. Two of the elements in the main transducer was mismatched in polarity and caused the beam pattern according to figure 29 in section 12.2.1. To account for the error, the electrical polarity was changed by inverting the driver signal and analog input on the Field Programmable Gate Array (FPGA) hardware for the two inverted channels. The test transducer was not tested for polarity. Furthermore the polarity of the test modem lack the multi channel reconfigurable hardware and polarity needs to be implemented correctly on transducer level.

9 Electronic design

The electronics was implemented using a modular design where several daughter boards dock into a motherboard as illustrated in figure 8. The daughter boards consists of a Power Supply Unit (PSU) that supplies the system with power and six Channel boards which provides electrical amplification for both transmission and reception of acoustic waves. A data acquisition platform is connected to the motherboard which controls the system and samples data. A full manufacturing of all boards for a modem requires a workload of approximately a week, however a single channel board or PSU can be completed within a half day of work. Additional iterations of manufacturing in the development may be required due to design errors, manufacturing errors or damaged components. The modular design was chosen to reduce the manufacturing time during development due to these errors and damages. Furthermore, a modular design allows for simplified Component testing.

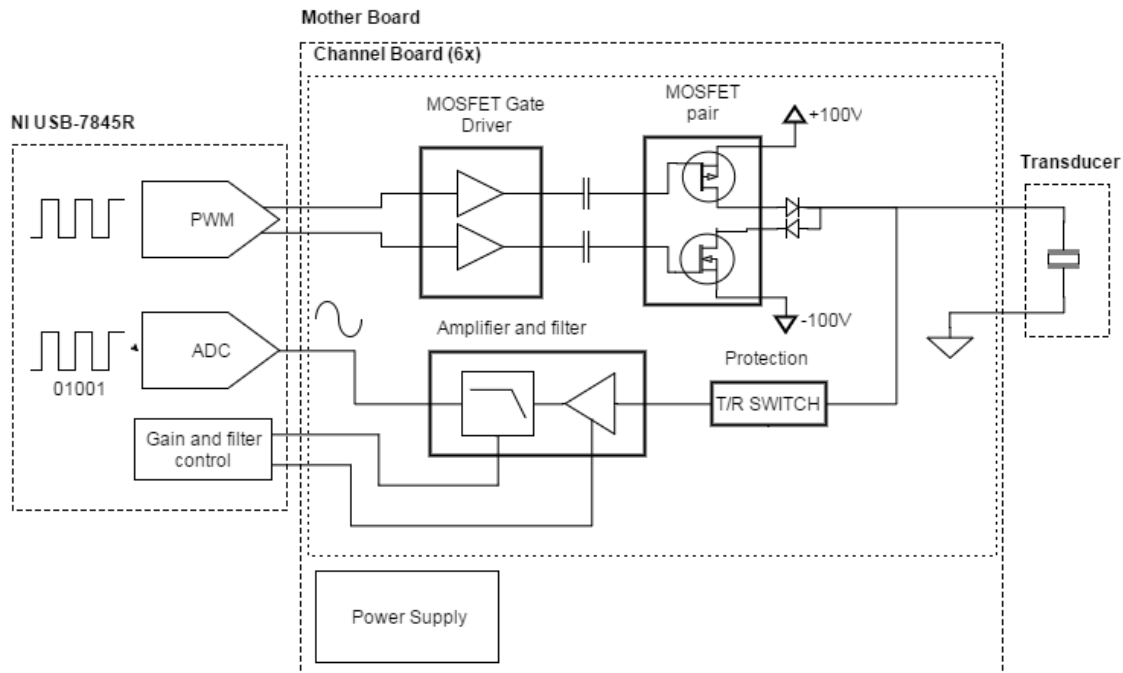


Figure 8: A diagram describing the complete electrical system. The Channel board and Power supply docks into the Motherboard and the data acquisition platform is connected through a cable. The transducer array are connected to the Channel boards through SMA-cables.

9.1 NI USB-7845R

The NI 7845R is an USB data acquisition platform with Analog-to-digital converter (ADC), Digital Input Output (DIO) and FPGA [30]. The FPGA is needed to perform high speed signal processing for filtering, resampling and beam forming. The data acquisition platform was chosen due to its ADC properties and FPGA size-and components. There are 8 on-board ADC's which provides synchronous sampling at $500k\text{Sample/S}$. Having synchronous ADC's is important as models for beam forming assumes no relative phase shift introduced in the receiving stage.

9.2 Motherboard

The motherboard provides an interface between power supply, Data Acquisition (DAQ) platform and channel boards. It contains two LM339 comparators from Fairchild [31] to level shift the DIO's on the DAQ platform from 0 and 3.3V logic to $\pm 5V$ logic on the channel boards. The comparator threshold is set to $1.65V$ by voltage division from the $5V$ source. The 7845 connects to the motherboard by a shielded cable. Figure 9 show the assembled motherboard.

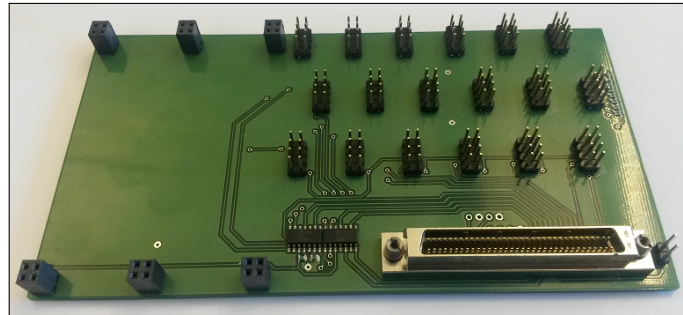


Figure 9: Picture of the manufactured Main modem motherboard. Six channel boards and the Power supply docks into the motherboard. The PCB was assembled at Mälardalen University.

9.3 Power supply

The power supply shall provide a stable $\pm 5V$ source for sensitive signal circuits and a $\pm 100V$ source for the piezo drivers. The transmission and receiving shall not occur at the same time and hence the $5V$ supply can be designed for stability during low load on the $\pm 100V$ supply.

The implemented design of the PSU is illustrated in figure 10. The $\pm 100V$ stages are con-

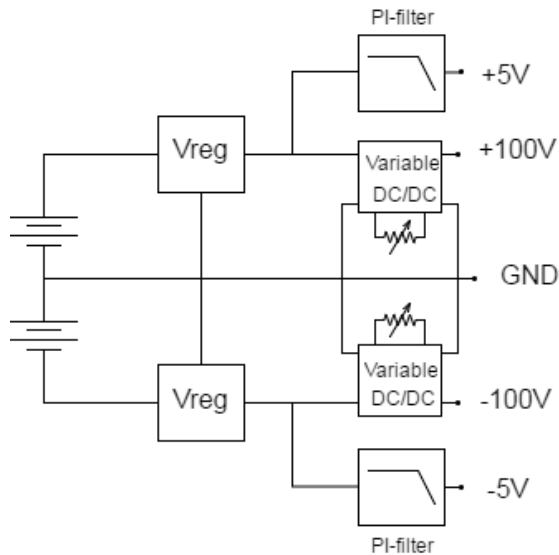


Figure 10: Diagram of the Power supply design. Two linear voltage regulators are used to supply sensitive circuits with electricity while two switched DC/DC regulators supplies power to the high voltage piezo driver stages. Two PI-filters are used to filter noise generated by the DC/DC regulators.

nected in series with the $\pm 5V$ stages. This is because the $\pm 100V$ stage requires a $\pm 5V$ input source. The $5V$ stage consists of 2 linear voltage regulators from Texas Instruments [32, 33] to provide low noise on the $5V$ channels. Linear regulators were considered feasible for the application as the effect loss is small due to the low difference in voltage between input and output. The $\pm 100V$ was implemented using switched DC/DC converters from Recom [34] working at $200kHz$. Output level can be lowered to $\pm 50V$ using a potentiometer. A PI-filter, depicted in 11, was implemented between the stages to insulate the noise from the switched DC/DC to the $5V$ line. The manufactured PSU is depicted in 12.

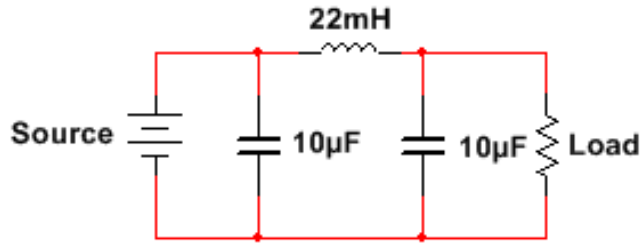


Figure 11: The implemented PI-filter used in the Power supply to remove noise from switched DC/DC converter.

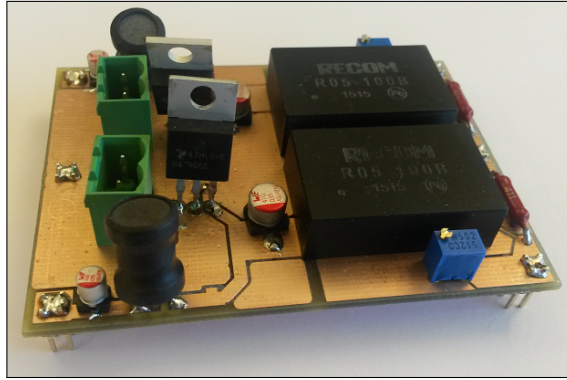


Figure 12: Picture of the manufactured Power supply. The Power supply docks into the Motherboard. The board was manufactured and assembled at Mälardalen University.

9.4 Channel board

The channel board can be divided into a transmitting and receiving part. The transmitting circuitry uses a complementary N- and P-channel Metal Oxide Semiconductor Field Effect Transistor (MOSFET) transistor pair and a high speed dual MOSFET gate driver from Supertex inc [35, 36] to amplify PWM signals to the piezo elements. In the receiving circuitry of the channel board there is a digitally controlled anti aliasing filter and 4-Bit programmable gain amplifier from Linear Technology [37] to filter and amplify the received signal before analogue to digital conversion. The very sensitive amplifier is protected from the high voltage driver through a T/R (Transmit/Receive) switch from Supertex inc [38]. One of the manufactured channel boards are depicted in 13.

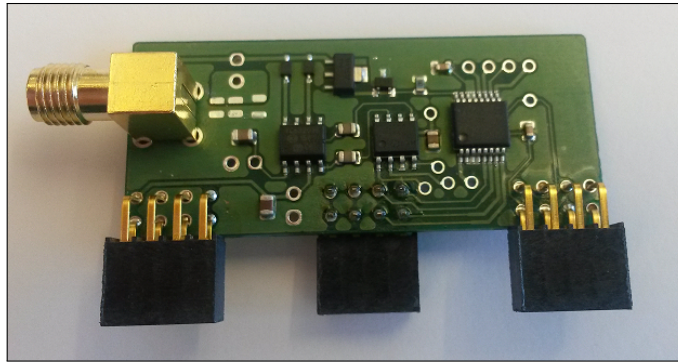


Figure 13: Picture of the assembled Channel board. The board connects to the Motherboard through the vertical headers. The SMA connectors connects to the piezo elements of the transducers. The board was assembled at Mälardalen University.

9.4.1 Piezo Driver

The piezo elements are driven by PWM signals that are amplified from $0 - 3.3V$ to the output voltage of the PSU at $50 - 100V_{peak}$. The square wave produces harmonics at multiples of the signal frequency. These harmonics are damped by the transmitter and the capacitive and electromechanical properties of the piezo elements. Harmonics are also damped by the acoustic channel and the receiver which has an 8th degree low pass filter in the amplification stage. These properties makes the PWM based approach a feasible design to drive the piezo elements. PWM based drive has the advantage of reducing the implementation complexity of the electronics and system design.

The MOSFET driver stage is implemented using a half bridge configuration where the MOSFET gate driver shift the level of PWM to the desired source-gate voltages of the MOSFET transistor pair. The shifted levels are designed to fully close and open the transistors, this occur when $R_{ds(on)}$ is considered saturated. The P-MOSFET has a drain-source resistance of $R_{ds(on)} = 10\Omega$ when gate-source voltage is $\Delta V_{gs} = -4.5V$. Additional gate-source voltage have little effect on the resistance and hence $\Delta V_{gs} = \pm 5V$ was chosen for the N-and P-MOSFET driver. Between the MOSFET driver and the MOSFETs gates, two capacitors are connected in series causing the controller only to work in continuous switching mode, this design removes the possibility to short circuit the bridge due to unexpected DC input. The design uses a common signal to drive the gate voltages, this simplifies the control but causes a small “no load” current to flow through the transistors. The current was measured and presented in the results section. An optional electrical filter was placed at the output to the transducer. The filter can be used to reduce harmonics by changing the output impedance.

9.4.2 Relaxation of piezo elements

The half-bridge design allows for connecting the piezo to $V+, V-$ or to be left a floating state. The design does not allow forced relaxation of the piezo voltage by ground discharging. This is of importance as the piezo voltage in receive mode is assumed not to be affected by the previous driving voltage. To meet this assumption, relaxation to a voltage level which can be considered negligible has to occur. The actual relaxation time t_{rel} was estimated in floating state and considered when designing the idle period in the communication flow.

9.4.3 Amplifier filter and protection

The amplifier gain is variable between between 1 to $16V/V$ which makes the system less hardware dependant as it obtains a wider dynamic transmission range. The amplifier stage includes an anti aliasing 8th degree low pass filter with variable cutoff between 0 to $150kHz$. The variable cutoff filter enables the usage of elements with different working frequencies. The amplifier and filters on the channel boards are commonly controlled by the output from the comparator level switch on the motherboard and can hence be controlled by FPGA hardware. The received carrier strength and frequencies are assumed to be equal at the amplifier input stage and no difference is made on electrical level for the hardware channels. Having individually controlled cutoff frequencies between the channels will cause relative phase shift between them. This phase shift causes the model of digital beam forming to fail unless compensated for. The amplifier circuit is protected using the T/R (Transmit/Receive) switch. The switch produces a high impedance against voltage higher than $\pm 2V$ signals while functioning as an 15Ω resistance at lower voltage. This keeps the voltage input to the amplifier stage within maximum input voltage range.

9.5 Noise considerations

The Switched DC/DC converter induces noise at the switching frequency as well as harmonics. The DC/DC converter was chosen to operate at a frequency of $200kHz$ which is higher than the frequency of the carrier signal. By this design, the noise can partly be damped in the anti-aliasing filter, however correct DC/DC filter design, ground return path and PCB layout is critical to reduce noise of the received carrier signal. The ground return path for analog signals was separated from the ground of the high voltage piezo driver in the design of the Motherboard, Power supply and

Channel board. Early experiments during design showed that proper separation could reduce noise between ground and $\pm 5V$ supply by a factor of 10. The goal of the motherboard layout was to keep the sensitive analog signal processing separated from the high power circuitry. A ground plane was used to shield the signal traces going to the ADC. Filtering of low frequency EMI (Electromagnetic Interference) such as 50Hz noise from light bulbs was not included in electronics design but optional to implement on FPGA hardware using Hardware Description Language (HDL).

9.6 Test modem

A second modem, referred to as the “Test modem”, was developed to test the beam forming, localization and communication program on the Main modem. The Test modem was designed to receive and transmit communication with an omnidirectional pattern and not perform any localization. In order to reduce complexity of the project the modem was kept very similar in design to the Main modem. Both channel boards and PSU was compatible with the test modem. The modular design was maintained, however the phase array constellation was rearranged to provide omnidirectional beam pattern.

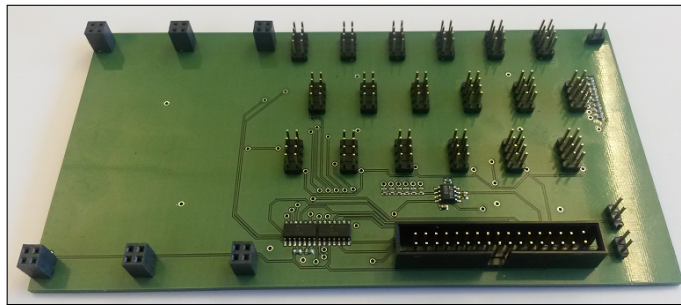


Figure 14: Picture of the manufactured test modem motherboard. Six Channel boards and the Power supply docks into the motherboard. The PCB was assembled at Mälardalen University.

9.6.1 MyRIO

The hardware platform MyRIO [39] from National Instruments was used for the test modem. The hardware platform was available at MDH and was used to reduce the cost of the project. The MyRIO platform has a single ADC which can run at 500kS/S. The MyRIO FPGA is integrated into the Xilinx Zynq-7010 System on Chip (SoC). The FPGA has just enough slices and block Memory to perform the required tests after performing the following optimizations.

1. Removing front panel objects in labVIEW to save space
2. Using just enough long queues on target to save block memory
3. Shorten Direct Memory Access (DMA) queues which are implemented using slices and pass the element into target-scoped queues which can be implemented using block memory

9.6.2 Electronics design

As the Main modem design required multiple synchronous ADC's and digital beam forming, the electronics was redesigned to sum the analog signals from the amplifiers into a single channel which can be sampled by a single ADC. With a single ADC, and needs of expensive synchronous ADC's are removed. Summing the signals assumes that the elements of the array in the test modem does not experience TDoA to the degree that the sum of the channels signals is subjected to strong negative interference due to relative phase shift between signals.

Summing sinusoids of the same frequency causes a result shifted in phase and amplitude depending on the original amplitudes and phases. For small values of TDoAs, the relative phase shifts are small and causes strong positive interference near maximum. The resulting phase shift

is time invariant which is of little importance for the resulting signal when using the modulation scheme Differential Phase Shift Keying (DPSK). The TDoA can be assumed small with the current arrangement of the test modem. This is due to that the length of the test transducer is much shorter than the distance between the transducers and that the test transducer is placed vertically towards the Main modem. Analog voltage summation was implemented using an operational amplifier. The amplifier was chosen so that slew rate met the following condition. $SlewRate > 2 \cdot \pi f V_{peak} = 2 \cdot \pi \cdot 10^5 \cdot 10 \cdot 10^{-6} = 6V/\mu s$. The LT6202 [40] low noise operational amplifier from Linear Technology with Slew rate $12\mu V/s$ was used. The inverting and non inverting summation circuit was tested, the noise level was reduced when in inverting mode and ultimately chosen for the final design.

9.7 Lessons learned

The largest pitfall in the project was manufacturing of the electronics. 4 weeks was spent in the lab having only 40% production yield. The process of manufacturing included setting via's by soldering pins from hole mounted resistors on both sides of the PCB. The errors was most often caused by vias not properly conducting. Some of the errors was due to not having a soldering mask which caused the PCB's to be very sensitive to short circuits between traces with thin clearances. In order to complete the manufacturing process, PCB's were ordered including soldering masks. The following manufacturing attempts had a 100% production yield.

A few design errors were encountered. The protection switch for the channel boards was successfully tested in the design phase. During Channel board integration, the component grounded the load which caused short circuit during the low voltage period. The error was that the "COM" pin which was supposed to be left floating was grounded, unfortunately this error was not raised in the previous iteration.

The comparator circuits required external pull up which was not specified clearly in the data sheet. These two design errors were based on assumptions and could have been avoided being very thorough when looking into how to use the components. Another error was related to file management such as having multiple versions of the same file. Very much time was spent troubleshooting PCB manufacturing errors such as non conducting vias. This can be avoided by ordering PCB's from a professional manufacturer, additionally they can provide a soldering mask to increase the quality of the PCB through the manufacturing and usage life cycle.

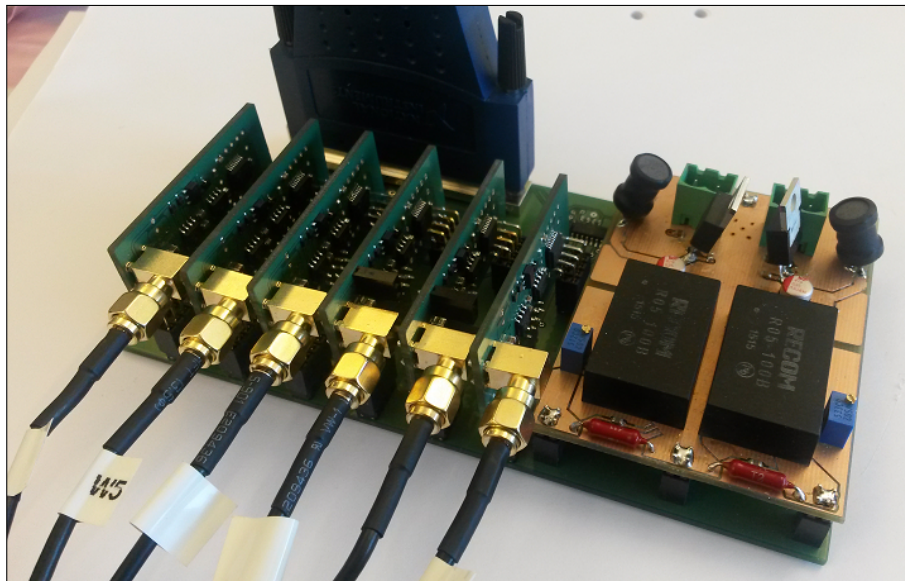


Figure 15: The complete Main modem with Power supply, Channel boards and cable to the data acquisition platform. The SMA cables connects to the transducer array.

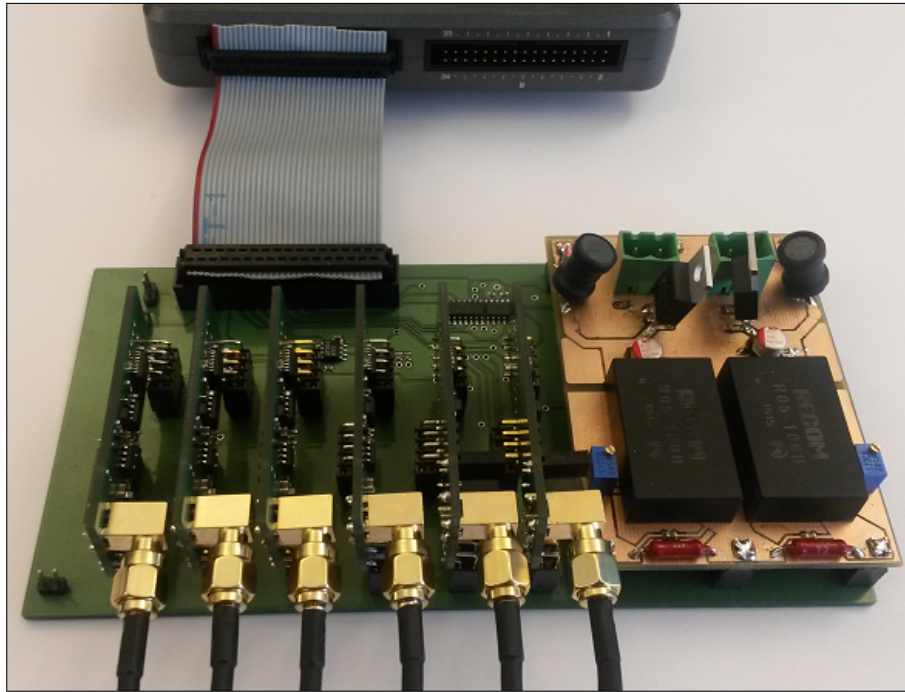


Figure 16: The complete test modem with Power supply, Channel boards and myRIO platform. The SMA cables connects to the transducer array. The hardware platform MyRIO was used to reduce cost of the project and simplifications was made accordingly.

10 System design

The following design was used for the Main modem. The design allows for developing of a communication and localization system on PC without losing the valuable FPGA properties such as timing and high throughput digital signal processing. The system was developed in LabVIEW which includes a large library of code and analysis tools.

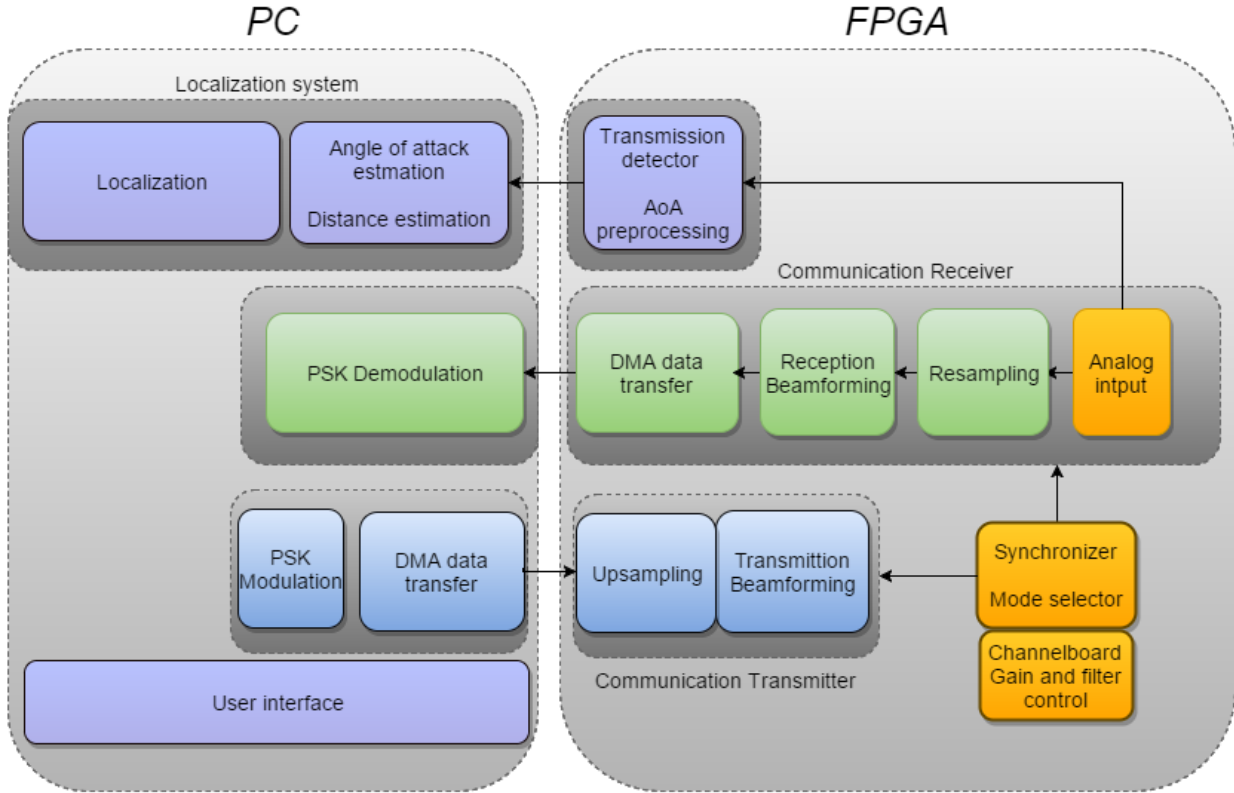


Figure 17: Software overview. A PC was used to perform localization and communication modulation/demodulation tasks. An FPGA was used to perform operation which requires high throughput and a high level of timing such as high sampling analog input from the elements and drive the piezo elements. DMA was used to data transfer between the PC and FPGA.

10.1 Digital beamforming

Beamforming is the technique of using an array of antennas to obtain a spatial filter for transmission and reception. The direction and properties are adjusted by weighting and phase shift the received signals. The process can be done in time domain and frequency domain. The signal can be transformed to frequency domain using FFT. In frequency domain the signal weighting can be done using multiplication with a complex weight and the interesting fourier bin. The data is phase shifted by the angle of the complex weight and scaled with the magnitude of the number. After weighting the signals they are added and transformed back to time domain using Inverse Fast Fourier Transform (IFFT).

In time domain the technique can be implemented using a digital delay line queue for each of the different signal channels. The elements chosen from each channel for summation is selected based on the queue position. This corresponds to delaying the elements. This technique is referred to as “delay and sum”. Delay and sum was chosen for beamforming due to simplicity and low FPGA resource usage. Additionally the method can be used for beamforming in both transmitting and receiving mode.

10.1.1 Geometry analysis of beamforming

Figure 18 describes the geometry of TDOfA between elements assuming planar wave and single point transducers. The elements are indexed by $N = 0, 1..5$. From the figure, equation 14 is derived,

$$l \sin(\theta) = c \Delta T \quad (14)$$

where c is the speed of the incident wave c with an angle θ . ΔT is the time difference of arrival

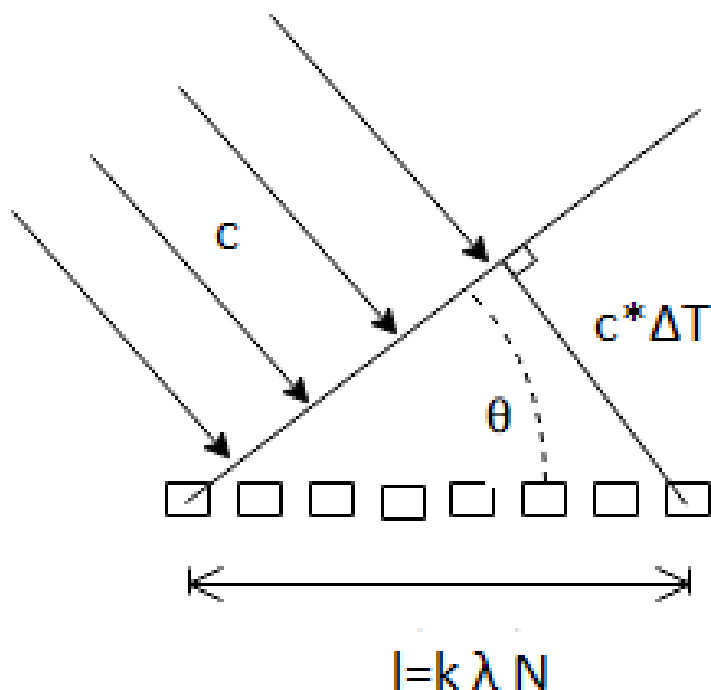


Figure 18: TDOfA (Time Difference of Arrival) between receiving element of an incident wave with an angle θ and a speed c . Index number 0 is the first element to the left.

due to an increased travel distance a . ΔT can be expressed as a phase shift ϕ of the incident wave form with a period T . l is the distance between two elements in the array and is described in detail

in equation 16

$$\Delta T = T \frac{\phi}{2\pi} \quad (15)$$

The displacement between elements can be defined as a scaling variable: k of the wavelength times the number of elements. In our case, k was selected to 1/2.

$$l = Nk\lambda = NkcT \quad (16)$$

Using the equations 14 and 15 we get that

$$lsin(\theta) = cT \frac{\phi}{2\pi} sin(\theta) \quad (17)$$

By solving equation 17 for phase, equation 18 is obtained.

$$\phi = \frac{2\pi lsin(\theta)}{cT} \quad (18)$$

Inserting equation 16 into 18, the phase simplifies to

$$\phi = Nk2\pi * sin(\theta) \quad (19)$$

or inversely

$$\theta = arcsin\left(\frac{\phi}{Nk2\pi}\right) \quad (20)$$

This equation allows for estimating the phase shift occurred between elements in the phase array.

10.1.2 Beam forming in the digital domain

The following sections discusses how to design a beam former in the digital domain on FPGA hardware. Resolution due to quantization and how to chose a resampling factor on the FPGA is considered.

10.1.3 Resolution and sampling rate

A limitation when designing a delay and sum beam former is the resolution in which elements can be chosen for summation. The resolution depends on the ratio between signal frequency and sampling frequency $n = \frac{F_s}{f_0}$ and is given in degrees by $\theta_{min} = 360/n$. If a signal of 40kHz with a sampling to signal factor of 10, a resolution of $360/10 = 36^\circ$ is achieved. Figure 20 illustrates the error due to quantization.

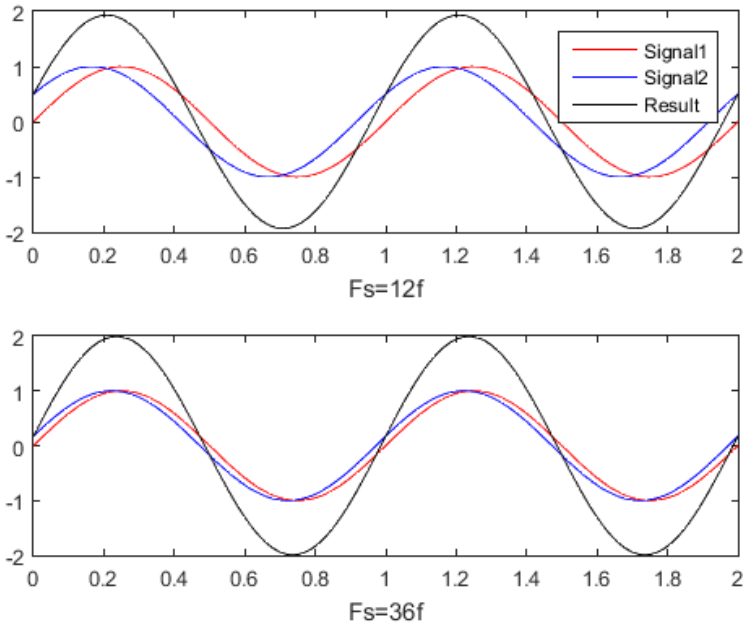


Figure 19: Error when summing sinusoids due to quantization. The error causes a phase and magnitude shifted result. The significance of the error depends on the ratio between sampling and signal frequency.

Figure 20 shows the maximum error due to quantization of 2 channels based on a sampling to signal ratio of 12 and 36, the result is a phase shifted signal with an amplitude slightly less than sum of the original sinusoids. A desired minimum signal sampling rate was chosen to $F_s = 36f_0 = 3.6MHz$. At a sampling to signal ratio of 36, the resulting amplitude is reduced by less than 1% and the resulting phase shift is approximately 4.6 degrees. A technique to increase the sample rate with little effect on the signal spectrum is in signal processing referred to as interpolation. Interpolation can be achieved by first perform zero stuffing to increase the number of samples and then apply lowpass filter to remove high frequencies introduced by the zero stuffing.

10.1.4 Phase shift and sampling rate

In order to perform beam forming in the digital domain, it is desired to model the relation between TDoA and phase shift in the discrete domain. Specifically it is desired to determine how many samples that is required to phase shift a signal channel for reception or transmission. The number of samples to shift a signal can be expressed as a function of Angle of Attack, spacing distance, sampling rate, speed and frequency of incoming signal. Using this expression, the queue elements for summing can be selected.

The time shift due to phase shift is given by

$$\frac{\phi}{2\pi}T = T_{shift} \quad (21)$$

When sampling the signal with a sampling period T_s a number of samples of $n_{shift} = \frac{T_{shift}}{T_s}$ will be processed in the beam former. By inserting T_{shift} into 21, equation 22 is obtained.

$$n_{shift} = \frac{T_{phi}}{2\pi T_S} \quad (22)$$

Finally equation 19 is inserted into 22 which gives equation 23

$$n_{shift} = \frac{TNk2\pi\sin(\theta)}{2\pi T_s} = \frac{TNksin(\theta)}{T_s} \quad (23)$$

In order to store elements in a queue containing elements of the upsampled signals required to achieve a beamforming with $\pm 45\text{deg}$ a Queue of $n = \frac{\Delta T}{f_s} = \frac{66\mu\text{s}}{0.28\mu\text{s}} = 236\text{elements/channel}$

10.1.5 Implementation on FPGA

Queuing can be implemented using dedicated FPGA memory blocks, external DRAM or using slices. The elements queued were of size 32 bits. Block memory was chosen as it provides efficient hardware utilization for data queuing and allows for read and write operation within a single clock cycle. Dynamic random-access memory (DRAM) was not selected as it cannot be used for single cycle read and write operations. There were not enough slices available in the hardware to queue the raw data for all 6 channels.

10.2 Localization

The following section describes the task of localizing underwater acoustic modems and is divided into measurements and localization algorithm. The measurements techniques was based on ToA and AoA to obtain distance and angle towards an acoustic source. The localization algorithm was based on EKF to track other modems assuming static targets.

10.2.1 Distance measurement

Measuring the distance between the acoustic modems was based on ToA in a synchronized system. Distance measurement was implemented on the FPGA and conversion to meter was implemented on the PC. The Range detection of an incoming signal was initially performed by an Root Mean Square (RMS) calculator together with a threshold. If the RMS on a received channel exceeds the threshold, the signal is considered received. The RMS was measured from the analog input of a single element in order to achieve omnidirectional perception for the detector and not to utilize beamforming to detect a signal. The analog input bypasses the interpolation circuits used by the beam forming circuit to maintain fast response time when receiving a signal. The input to the RMS measurement used a Hanning window with a size of 3 signal periods. The RMS component was later changed to only perform thresholding, however a high pass filter was added to remove the DC signal offset. The design change was performed to simplify the solution, additionally the solution showed to be less dependant on adjusting the threshold level to properly detect an incoming acoustic wave and reject noise. A 40MHz counter was used to estimate the range to the Test modem, the RMS detector triggers the counter block to output the current counter value upon signal detection. Each new reading was sent to the Personal Computer (PC) which converts the counter values to distances in meter using formula 24,

$$\text{distance} = \frac{C_{\text{counter}}}{40 \cdot 10^6} \cdot c - o \quad [\text{meter}] \quad (24)$$

where $40 * 10^6$ is the FPGA clock speed, $c = 1480\text{m/s}$ is the speed of sound in water and o is the systematic detection time offset (initially set to 0).

10.2.2 Angle of Attack

In section 10.1 a model for beam forming was described and equation 19 related a phase shift to the angle of an incident wave. If the phase shift can be measured, the incident angle of a received waveform the can be estimated. The absolute phase was measured using an FFT based approach. The phase difference is generally ambiguously defined as there exists more than one solution for the phase difference between two angles. The problem was solved by an algorithm which is trying to find the minimum phase difference between two elements. The approach is feasible as the maximum detectable angle in the specification is set to 45° . Only one phase difference is required to estimate the AoA, however using the phase shift between all adjacent array elements the system can provide a better estimate. The following block diagram shows how a number elements can be used together to increase the accuracy of estimation by averaging. The phase difference was used to estimate AoA by inverting the equation 19.

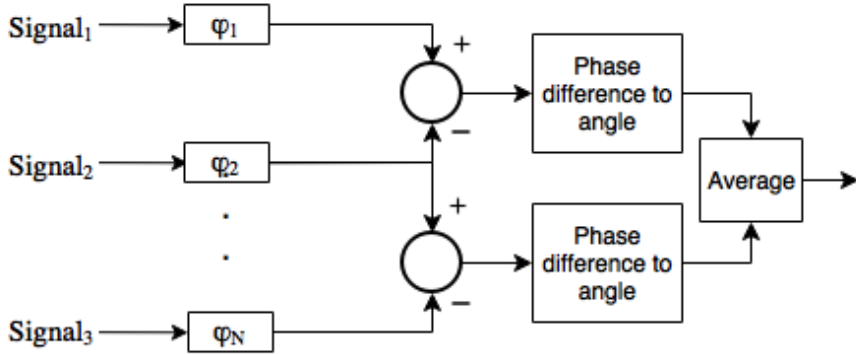


Figure 20: Phase shift estimation. Phases was estimated using FFT to find the frequency of the strongest frequency component. The minimum phase shift was calculated between the elements. A model was used to relate the phase difference to the incident angle. The estimated angles were averaged.

10.2.3 Localization algorithm

Extended Kalman Filter was chosen as a basis for localization. The method can be used to estimate the state of a set of robots. The algorithm was used to estimate the state position vector given by equation 25

$$X_t = [x \ y]^T \quad (25)$$

Even though the strength of the filter is to estimate a dynamic process it can also be used to estimate a static process. The Extended Kalman Filter is included in this thesis as it provides a basis for further work on a localization system. Kalman filter is optimal given Gaussian measurement- and plant noise as well as a linear model. If the models are close to linear, EKF can be used by approximate the process or measurement model by the jacobian matrix. The equations 26 and 27 were used to filter the position.

$$\begin{aligned} \bar{\mu}_t &= \mu_{t-1} \\ \bar{\Sigma} &= \Sigma_{t-1} + R_t \end{aligned} \quad (26)$$

$$\begin{aligned} K_t &= \bar{\Sigma} H_t^T (H_t \bar{\Sigma} H_t^T + Q_t)^{-1} \\ \mu_t &= \bar{\mu}_t + K_t(z - h(\bar{\mu}_t)) \\ \Sigma &= (I - K_t H_t) \bar{\Sigma} \end{aligned} \quad (27)$$

μ is the state vector and Σ is the uncertainty covariance matrix for the state. R and Q are the noise covariance matrices for the process and the measurement. z is the measurement and $h(\mu_t)$ is the non linear mapping from state to measurement space.

H is the Jacobian matrix of the function $h(\bar{\mu}_t)$. For testing within this thesis, measurement space was set to state space and z and Q was represented in state space. z was converted to state space using equation 28, consequently H is represented by the identity matrix.

$$X_t = \begin{bmatrix} x \\ y \end{bmatrix} = \begin{bmatrix} r * \sin(\theta) \\ r * \cos(\theta) \end{bmatrix} \quad (28)$$

In equation 26 and 27, Σ and μ indicate predicted estimations and are not final filter output. The t refer to the iteration time step of the discrete update.

The filter is tuned by varying the elements in the covariance matrices R and Q which contain the variances σ_r and σ_θ on the diagonal.

The filter was initialized by the first measurement obtained from the acoustic sensor. Σ was initialized to a large value to allow for fast convergence towards the actual however not observable position vector. The tests was performed with plant and measurement noise presented in equation 29.

$$P = \begin{bmatrix} 1 & 0 \\ 0 & 1 \end{bmatrix} Q = \begin{bmatrix} 0.1 & 0 \\ 0 & 0.1 \end{bmatrix} \quad (29)$$

10.2.4 Synchronization

The main and Test modems were synchronized using a cable before pool deployment. The Main modem sends a pulse during the start of its sending time slot. The Test modem receives the pulse and start its receiving time slot upon the rising edge detection. Both hardware platforms uses a 40 MHz Clock for the FPGA. During testing, the need for a clock speed offset was discovered. Offset was implemented based on a counter to increase the synchronizer speed of the slowest node.

10.3 Communication

There are several different modulation schemes used in underwater communication systems. Among them are FSK and PSK which are the most common [2]. FSK is a non-coherent frequency modulation technique which uses a discrete set of frequencies to represent information. It is robust, reliable and easy to implement. PSK is a coherent phase modulation technique which modulates information by varying the phase of a carrier signal. PSK is capable of higher data rates but is less robust and requires more processing power due to the sophisticated algorithms needed [41].

While an implementation based on FSK modulation naturally can be considered a multi-carrier system PSK can be implemented either as a single carrier or as a multi-carrier system. Since the beamformer needs to be configured differently for each frequency a single carrier system reduces complexity and thereby becomes the natural choice.

10.3.1 Binary differential phase-shift keying

Since PSK is a coherent modulation scheme it requires the receiver to continuously track the phase of the transmitted signal. This is called carrier recovery and creates a reference signal which is used to determine the instantaneous phase of the signal. A variation of PSK is DPSK which modulates information as a relative difference in phase instead of an absolute difference. This illuminate the need for coherent detection which is a quite complex task to perform in underwater systems [41].

Binary DPSK is the simplest form of DPSK where information is encoded as either no change or as a 180° change in phase of the carrier signal.

10.3.2 Time Division Multiple Access

In order to enable communication between multiple nodes in a single carrier system some sort of mechanism is needed to share the medium. TDMA is described by Proakis and others [4] and is a channel access method which has been implemented to solve this problem. Every node in the network is assigned a time slot in which it is allowed to transmit data. The time slots were divided into $\frac{1}{16}$ of a second. Figure 21 illustrates the state transitions of the implemented TDMA subsystem. Each time slot are further divided into a localization period, a transmission period and a propagation period referred to as idle which is depicted in 22. During this thesis only two nodes were implemented which interchange roles as transmitter och receiver at each transition.

During the localization period, T_l , the transmitting node transmits a constant tone for 10 periods of the carrier frequency. The total overhead caused by the synchronization tone is estimated by equation 30. This tone is acquired by the receiving node and are used to calculate TDoA and

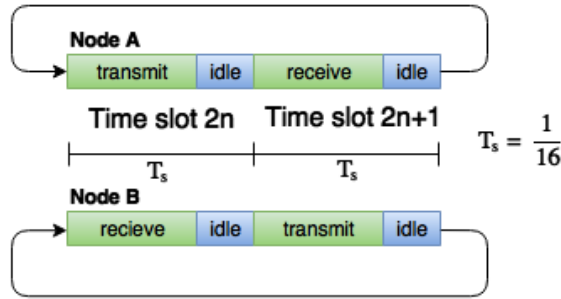


Figure 21: Illustrates the implemented TDMA protocol. The nodes interchanges roles as transmitter and receiver. The idle periods allows for propagation of the acoustic waves.

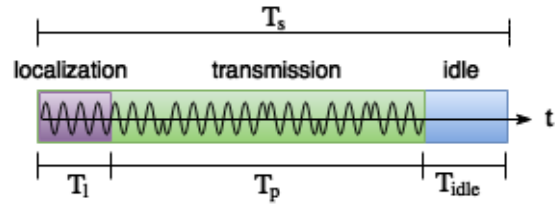


Figure 22: Illustrates how each time slots is further divided into a localization, transmission and idle period. During the localization period a localization tone is transmitted for AoA- and range-estimation. Data is transmitted during the transmission period and idle period allows for acoustic propagation.

AoA for localization, see section 10.2 for details. The duration of the period results in a total propagation spread of 0.375 meter, see equation 31.

$$100 \cdot \frac{T_{sync}}{T_{sym} \cdot T_{data}} \approx 0.78\% \quad (30)$$

$$L_{sync} = 10 \cdot T \cdot c \quad (31)$$

Where T is a period of the carrier wave and c is the speed of sound in water. The actual data is transmitted during the transmission period, T_p which is given by equation 32.

$$T_p = T_{sym} \cdot T_{data} \quad (32)$$

Where T_{sym} is the duration of each symbol and is expressed as a natural multiple of the period of the carrier wave.

$$T_{sym} = 4 \cdot T \quad (33)$$

During this period a single package consisting of 45 bytes in total are sent, see equation 34.

$$T_{data} = 8 \cdot 45 = 320 \text{ bits} \quad (34)$$

The purpose of the idle period, T_{idle} , is to allow for the acoustic signals to completely propagate between the communicating nodes. At its minimum the idle period needs to allow for the signals to propagate exactly the distance specified in the requirements which is 20 m. The idle period is calculated by equation 35

$$T_{idle} = T_s - T_p - T_l \quad (35)$$

Precise synchronization between the communicating nodes are necessary to properly utilize the time slots in TDMA [41]. In order to realize this a hardware is used to initially synchronize the nodes, see section 10.2.4 for details.

10.3.3 Transmitter

This subsection describes the process flow of how data gets modulated into a control signal that drives the piezo elements. The tx sequence generator subsystem encapsulates data into very simple packages. The DPSK modulation subsystem modulates data into the phase of a PWM carrier signal.

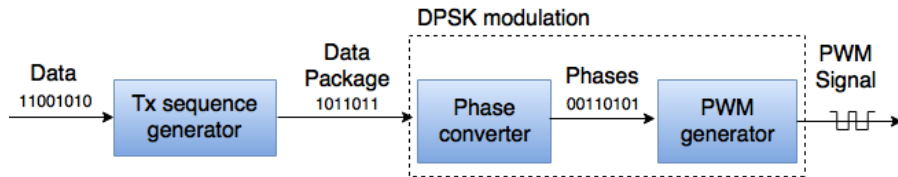


Figure 23: Diagram of the transmitter subsystem. The Tx sequence generator creates packages to be transmitted. The DPSK modulation subsystem creates the PWM control signal that drives the transducer arrays.

Tx sequence generator The Tx sequence generator takes data as input and creates packages to be transmitted. The packages consists of an initial synchronization pattern together with the data to be transmitted. The synchronization pattern are used by the PSK demodulator to determine optimal sample points for the symbols.



Figure 24: Illustrates the structures of the packages. The two byte sync pattern is used by the receiver to map phases to symbols. The remaining 43 bytes are actual data.

DPSK modulation The DPSK modulation subsystem is further divided into a Phase converter and a PWM generator. The Phase converter takes data as an array of booleans as input and modulates it into a sequence of absolute phases. A 0 is modulated as no difference in phase while a 1 is modulated by a 180° shift in phase. The resulting output is an array of booleans representing the two different phases of the carrier signal. The PWM generator creates the actual PWM signal that is going to control the piezo elements. It takes an array of booleans representing actual phases from the phase converter and modulates the phase of the control signal.

10.3.4 Receiver

The receiver part of the software is described in the sections below. The sampled signal is fed to a thresholder which removes weak, non relevant signals that occurs either before or after the signal of interest. The I/Q demodulation then converts the sampled signal to complex representation and feeds it to DPSK demodulation part which reconstructs the transmitted data.

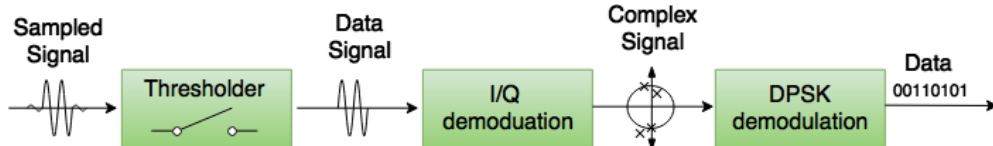


Figure 25: Diagram of the receiver subsystem. The thresholder functions as filter which separates weak non relevant signals from the actual transmitted signal. The I/Q modulation extracts complex data from the signal and the DPSK demodulator demodulates the signal to actual data.

Thresholder The thresholder is implemented using a fixed size window which sequentially calculates the absolute mean value of the sampled signal window by window. The purpose of the Thresholder is to remove everything but the signal of interest in order to reduce the workload for the rest of the receiver software.

I/Q demodulation In order to convert the sampled signal into complex representation an I/Q demodulation subsystem has been implemented. The signal is mixed together with two 90 deg phase-shifted sinusoids of the same frequency as the carrier wave. The resulting signals is then fed through a 6th degree butterworth lowpass filter with a cut off frequency set to approximately $\frac{1}{8}$ of the carrier frequency. The resulting outputs of the filters corresponds to the I/Q values of the complex representation of the signal.

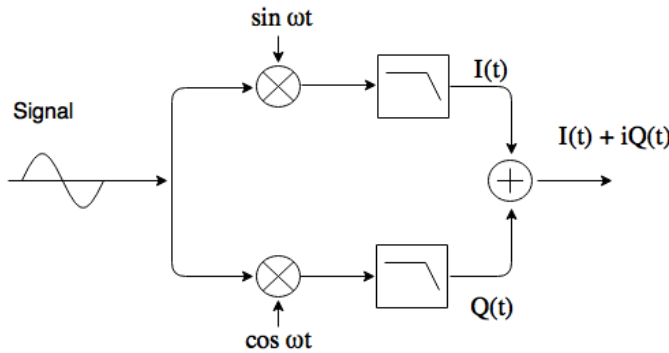


Figure 26: Shows the principles of the I/Q demodulation subsystem. The signal is mixed together with two phase shifted sinusoids which are then passed through two low pass filters. The outputs and then added to create the complex value that represent the signals I- and Q- values.

DPSK demodulation In order to demodulate the signal the receiver first needs to determine the optimal sample point of the signal. This is usually referred to as symbol timing recovery and is needed to obtain symbol synchronization. Any coarse frequency offset is removed from the signal before decimation is performed. The decimator uses the optimal sample point to down sample the signal to anything but the actual symbols. The sync sequence is then used to interpret and map the symbols and actual bits.

11 Testing

In order to verify that the requirements of the integrated communication and localization modem have been met a set of tests have been conducted. All tests that have required deployment in water have been performed inside a round pool with a radius of 2 m and height of 1m which is located within the schools facilities. To simplify the process a Test modem equipped with an omnidirectional transducer have been used to test the Main modem. All the hardware components of the main- and the Test modem are listed in tables 1 and 2. The tests are using either one or six elements in the respective transducer depending on the test. Early in the testing within pool environment it was found that continuous transmission causes a high amount of multipath and causes sporadic phase and magnitude changes of the received signal. All further testing was performed with pulsing.

For all minor tests which are not directly related to the requirements, a description together with the corresponding result is presented in section 12.

Quantity	Item
1	Directional transducer array
1	Main modem motherboard
1	USB-7845R
1	Power supply
6	Channel boards
6	SMA cables
1	PC

Table 1: A list of the components of the Main modem.

Quantity	Item
1	Omnidirectional transducer array
1	Test modem motherboard
1	myRIO
1	Power supply
6	Channel boards
6	SMA cables
1	PC

Table 2: A list of the components of the Test modem.

11.1 Test rig

In order to control and set the relative positioning and orientation between the two transducers a test rig has been built. The rig is shown in figure 27. The distance between the two transducer can be varied by adjusting the nuts of the four threaded iron rods spacing them apart. The angle between the transducers can be adjusted by rotating the rack on which one of the transducers are mounted as depicted in figure 28. The rack can be exchanged to an alternative rack which will turn the transducer from a horizontal to a vertical position. The drilled holes are used as incremental indicators of discrete steps of 3.9° between $\pm 45^\circ$. Due to manufacturing uncertainties the rack was observed to have a skewness causing the transducer to have an angular uncertainty of 3.5° . During the test the angular uncertainty was compensated by adding an offset to the observed angles. The precision of the test rig was approximated to $\pm 0.75^\circ$.

The test rig can be placed vertically with the test transducer on the bottom and the main transducer close to the surface. In vertical placement, part of the test rig is exposed to air and can be affected by wind. The rig can also be placed horizontally using floating boyus. The movement of the boyus can be affected by wind.



Figure 27: The rig was built at Mälardalens University. Two transducers are mounted with a distance spacing of 1m. The spacing distance and orientation between transducers can be adjusted by the test rig. An angular offset was detected in the test rig.

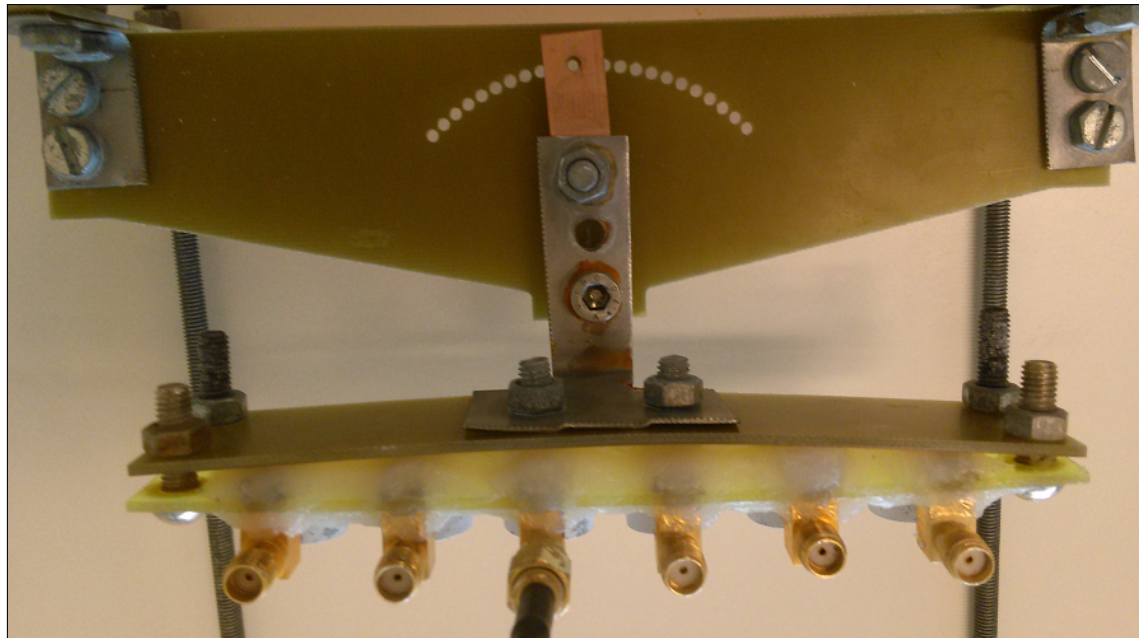


Figure 28: Close up picture of the rack on the test rig which allows for angular adjustments. A transducer is attached to the test rig.

11.2 Phase controllability test, T1

The beamformer was configured to transmit a set of signals for different directions. An oscilloscope was connected to two of the Main modems outputs to measure the relative phase of two sequent PWM signals. The minimum phase shift is limited by maximum clock speed which results in a resolution of 0.36° .

11.3 Beamforming transmission test, T2

The transducer of the Main modem was mounted to the variable rack of the test rig. All six transducers of the directional array was used to form the beam patterns. The transducer of the Test modem was mounted to the other static end of the test rig. Only one transducer of the omnidirectional array was used to receive the acoustic signals. The test rig was then deployed in the pool and the beamformer was configured to continually transmit pulses for a set of certain angles. For each of these angles the rack was varied between 0° and 30° . The RMS was measured and recorded to obtain the spatial filtering properties of the beamformer.

11.4 Beamforming reception test, T3

Directional reception of the beamformer was verified through a similar test to the beamformer transmission test. The transducer of the Test modem was mounted to the static end of the test rig. Only one transducer of the omnidirectional array was used for transmission. The transducer of the Main modem was mounted to the variable rack of the test rig. All six transducers of the directional array was used to receive the acoustic signals. The Test modem was then configured to continually transmit omnidirectional pulses. The rack was varied between -45° and $+45^\circ$ and the RMS was measured and recorded to obtain the spatial filtering properties of the beamformer reception.

11.5 Communication test A, T4

The two transducer arrays were placed inside an aquarium approximately 15 cm apart. Two transducers from each array were then connected to the USB-7845R data acquisition platform through the Main modem motherboard to simulate two communicating nodes. Data was transmitted using TDMA and binary DPSK.

In order to get an understanding of the magnitude and duration of the echo inside the aquarium, the received signal was sampled and analysed after amplification and transmission. As a reference the signal was compared to the transmitted pulse train.

11.6 Communication test B, T5

The two transducer arrays were mounted to the test rig 50 cm apart. One of the transducers from each array was then connected to the USB-7845R data acquisition platform through the Main modem motherboard to simulate two communicating nodes. The rig was then deployed into the pool and data was transmitted using TDMA and binary DPSK.

In order to get an understanding of the magnitude and duration of the echo inside the pool, the received signal was sampled and analysed after amplification and transmission.

11.7 Angle of Attack test A, T6

The Main modem and the Test modem were mounted onto the test rig and placed vertically in the pool. The distance between the modems was 1m. The angle of the Main modem was adjusted from $-22,488^\circ$ to $+22,48^\circ$ by 13 evenly spaced steps. For each step the angle between the modems was measured by the Main modem 100 times.

11.8 Angle of Attack test B, T7

The Main modem and the Test modem were mounted onto the test rig and placed in the pool horizontally with the main transducer close to the edge of the pool and the test transducer and the test transducer located between the edge and the center of the pool. The distance between the transducers was 1m.

11.9 Localization test, T8

The Main modem and the Test modem were mounted onto the test rig and placed in the pool vertically 1m from the pool edge. The distance between the transducers was 1m. The angle of the Main modem was adjusted freely by the authors and the position was estimated, filtered and shown on the user interface.

11.10 Planar wave propagation test, T9

The models for beamforming reception and AoA estimation assumes planar wave propagation. However at short distances close to near field the model may not be valid.

In order to test the model, the test- and main model were placed at 1m distance pointing towards each other. Phases were estimated at the receiver and evaluated with respect to the shift depending on the index of the element. In order to increase the significance of the results in this test, the testing was performed in air. This medium causes the acoustic wave to propagate slower and reduces wavelength with a factor of $340/1480 \approx 0.23$.

12 Results

The following section presents results for the system and electronic tests. System tests are based on the setup described in section 11.

12.1 Phase controllability test, T1

Control phase	Measured phase
-54°	-54.72°
-36°	-36.0°
-18°	-18.0°
0°	0.0°
18°	18.0°
36°	36.0°
54°	54.72°

Table 3: Phase

Control phase	Measured phase
0.36°	0.351°

Table 4: Minimum Resolution

12.2 Beam forming transmission test, T2

The beamforming transmission test was conducted two times with different results.

12.2.1 Test session 1

A single set of measurements was obtained with 23 discrete steps between -45° and $+45^\circ$. The acquired beam pattern is illustrated in figure 29 where the angular uncertainty has not been compensated with the offset explained in section 11.1. The result is discussed in section 8.2.8.

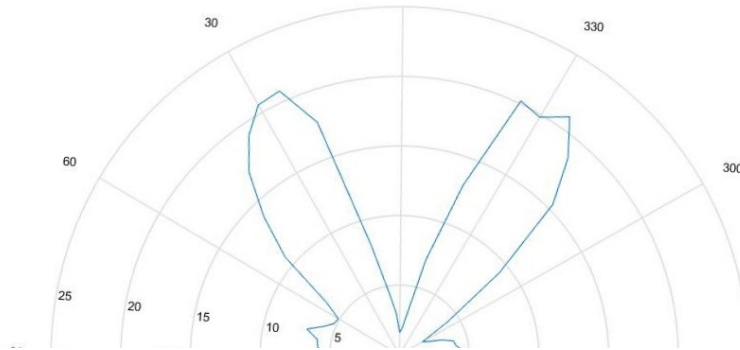


Figure 29: Undesired beamforming pattern caused by polarity shift of the piezo elements. The gain pattern has undesired grating lobes instead of a main lobe.

12.2.2 Test session 2

Five sets of measurements was obtained with 23 discrete steps between -45° and $+45^\circ$. The acquired beam pattern is illustrated in figure 30 and 30 where the angular uncertainty has not been compensated with the offset explained in section 11.1.

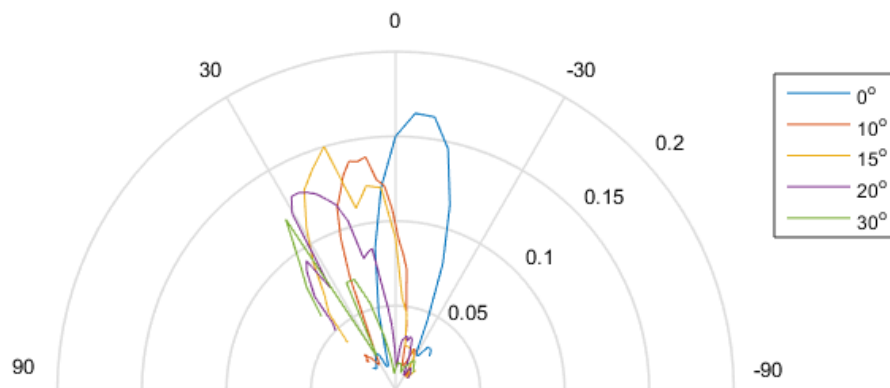


Figure 30: Beamforming transmission conducted for 5 different directions plotted in the same graph.

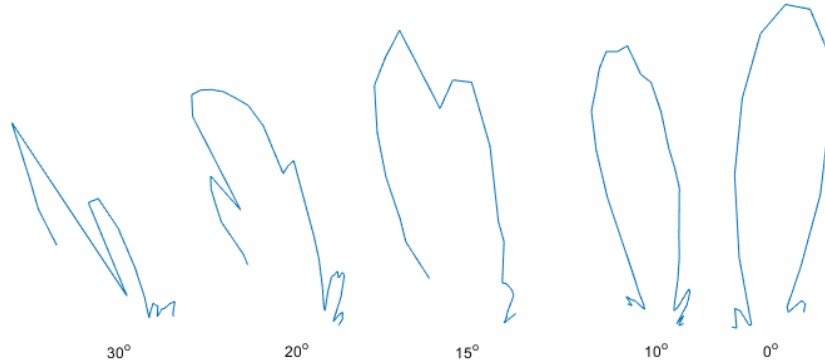


Figure 31: Beamforming transmission conducted for 5 different directions. Strength and shape change by the steered angle.

12.3 Beam forming reception test, T3

Two sets of measurements was obtained with 23 discrete steps between -45° and $+45^\circ$. The acquired beam pattern is illustrated in figure 32 where the angular uncertainty has been compensated with the offset explained in section 11.

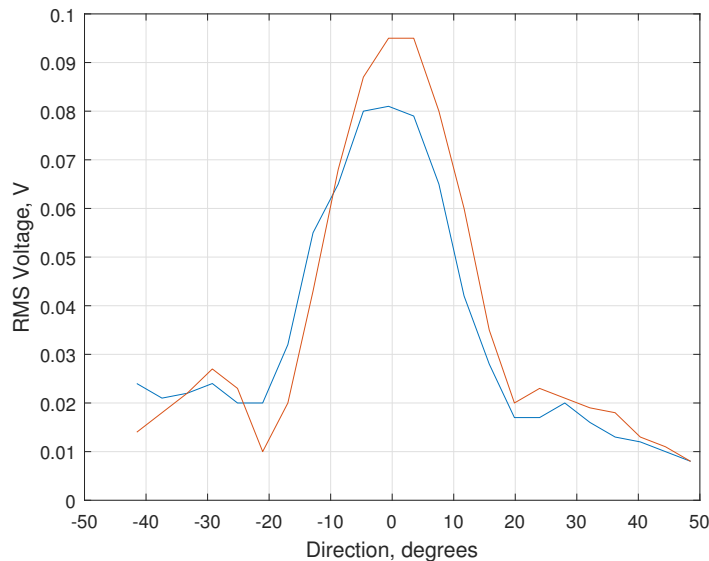


Figure 32: Beamforming reception. The RMS shown in the graph is based on the sum of voltage over the individual elements. The selected direction of beam forming is 0 degrees Red and blue describes the two set of measurements. Both graphs are compensated for offset.

12.4 Communication test A, T4

Data was transmitted successfully at a rate of $2.88Kbps$ with no bit error. The transmission was done under still water condition where the nodes were static. Any environmental change or movement of the transducers resulted in bit errors. Data transmission was only successful for certain unique alignments of the transducers.

Figure 33 shows how the carrier wave responds to phase modulation in the aquarium, the same signal is transmitted over a cable as a reference. Figure 35 shows a sequence the transmitted and

received signal. Figure 37 shows the extracted phase information from the same signal after the IQ-demodulation stage.

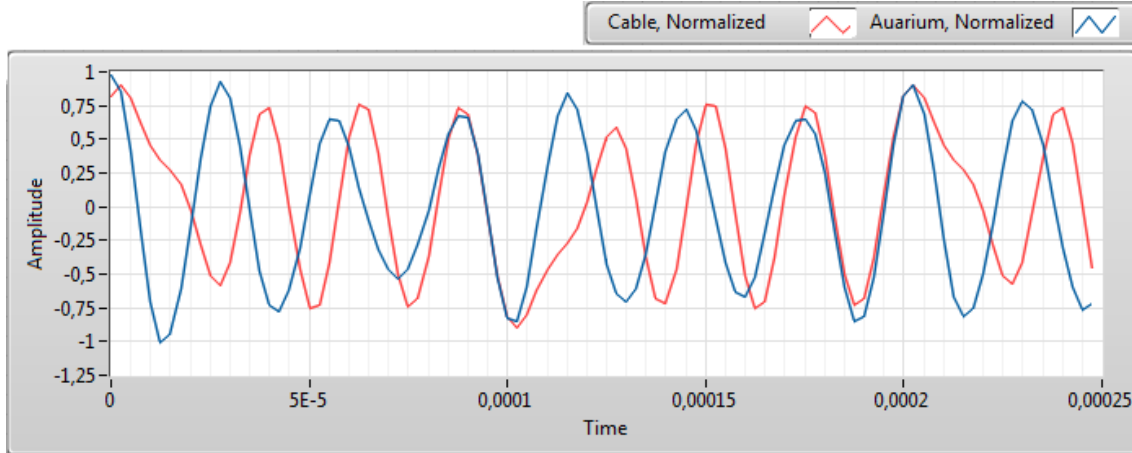


Figure 33: Phase modulation during transmission over cable and over an acoustic channel using the transducers. The phases are clearly shifted over the cable while the phases are slowly changed over the acoustic channel.

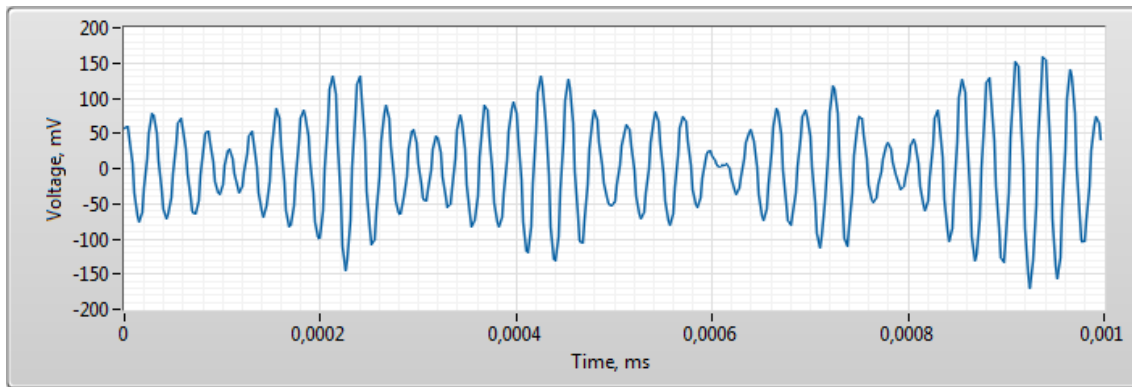


Figure 34: Data transmission over an acoustic channel inside an aquarium using binary DPSK. Data is encoded in the phase of the carrier signal. The figures shows a small part of a complete received signal.

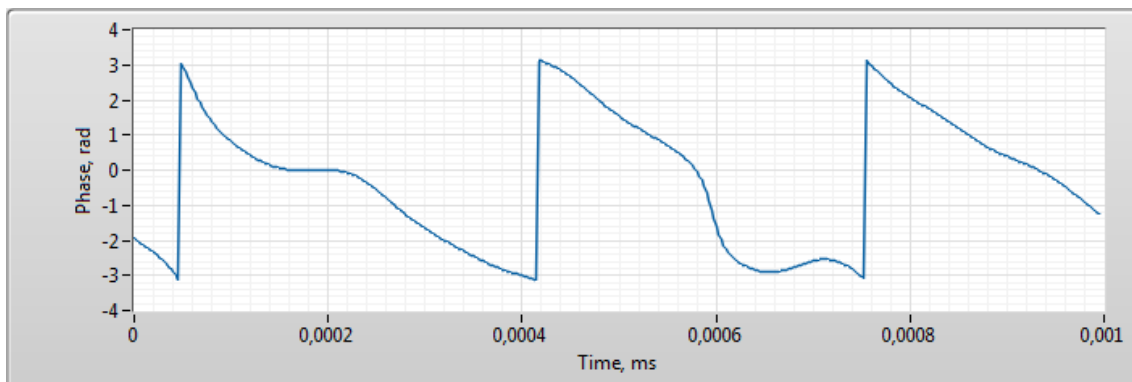


Figure 35: Data transmission over an acoustic channel inside an aquarium using binary DPSK. Data is encoded in the phase of the carrier signal. The figure shows the extracted phase from the I/Q demodulator for a small part of a complete received signal.

12.5 Communication test B, T5

Data was transmitted successfully at a rate of $0.64Kbps$ with no bit error. The transmission was done under still water condition where the nodes were static. Any environmental change or movement of the transducers resulted in bit errors, as did any increase in spacing between the two transducers. Figure 36 shows a piece of the received signal and illustrates how the carrier wave responds to phase modulation in the pool. Figure 37 shows the extracted phase information from the same signal after the IQ-demodulation stage. Figure 38 shows the complete transmitted and received signal. The received signal is still apparent after the signal transmission ends.

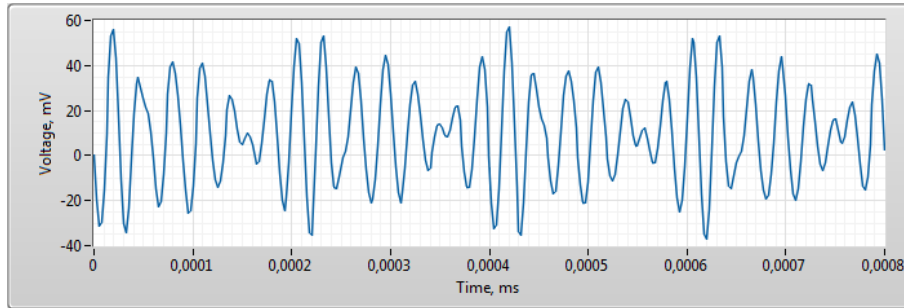


Figure 36: Data transmission over an acoustic channel inside a pool using binary DPSK. Data is encoded in the phase of the carrier signal. The figure shows a small part of a complete received signal.

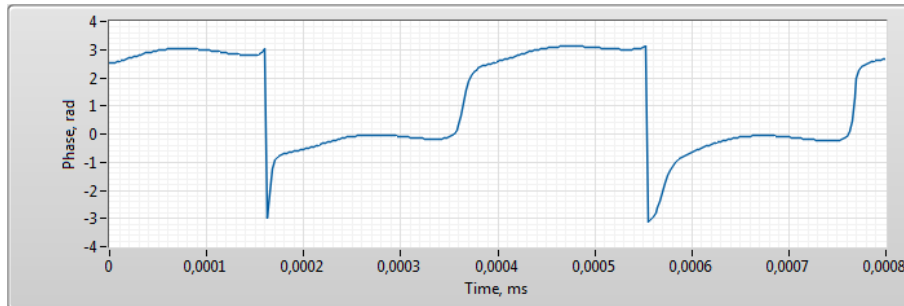


Figure 37: Data transmission over an acoustic channel inside a pool using binary DPSK. Data is encoded in the phase of the carrier signal. The figure shows the extracted phase from the I/Q demodulator for a small part of a complete received signal.

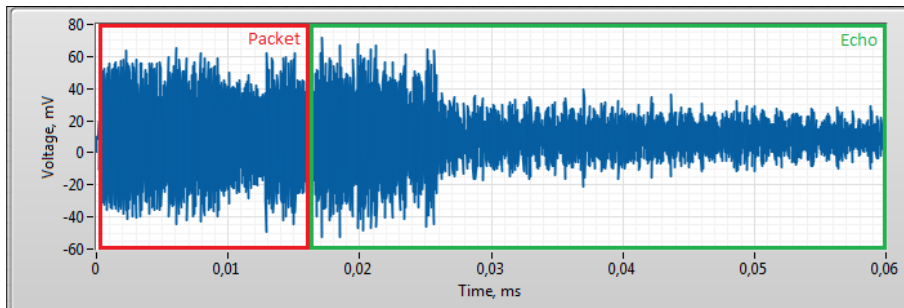


Figure 38: Shows a complete transmitted package and its echoes over an acoustic channel. The signal is recorded in a circular pool. The actual packet and echo are indicated by the red and green rectangular boxes.

12.6 Angle of Attack test A, T6

The test were performed 2 times and the results are shown in the figures 39, 40, 41 and 43.

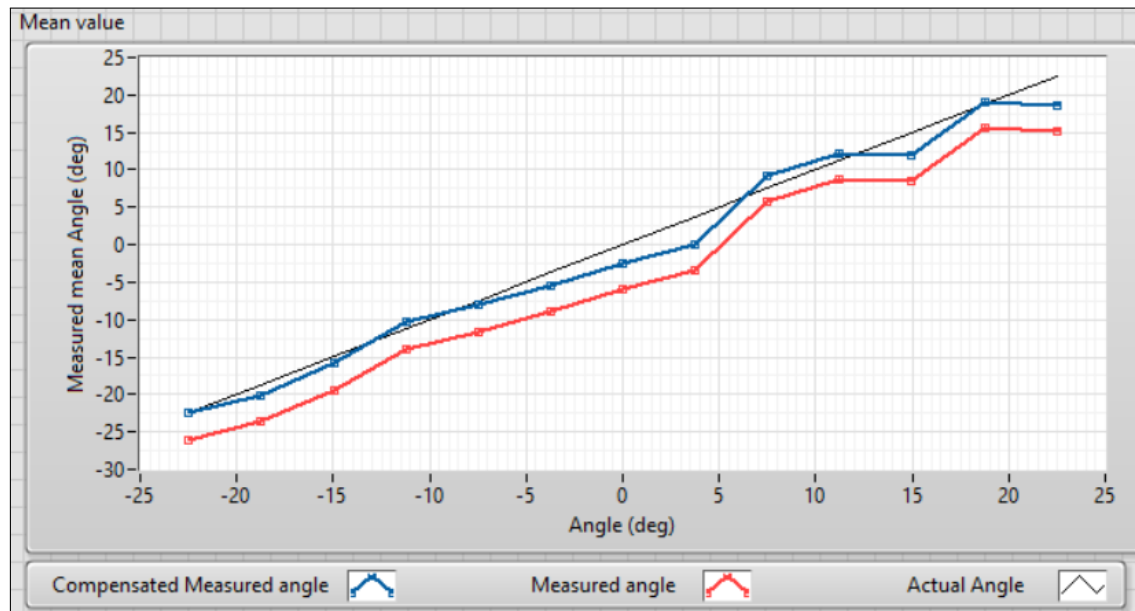


Figure 39: First data set. Black graph shows the actual angle. Red graph describes the measured angle. Blue graph describes the measured angle, compensated by the rig angle offset error.



Figure 40: First data set. Red graph describes the range of the measured angles. Blue graph shows the mean absolute deviation.

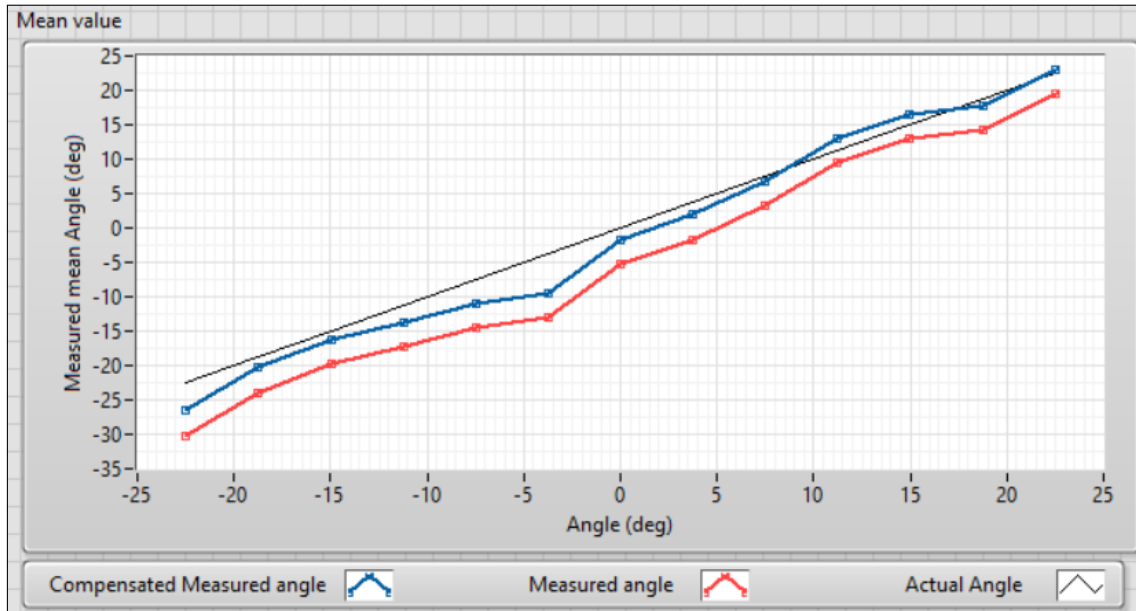


Figure 41: Second data set. Black graph shows the actual angle. Red graph describes the measured angle. Blue graph describes the measured angle, compensated by the rig angle offset error.

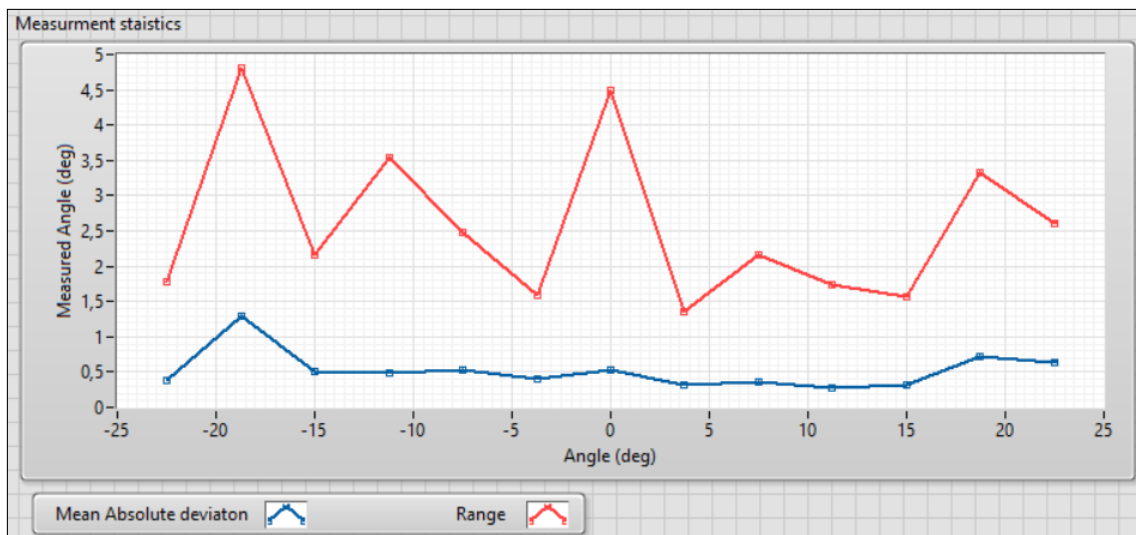


Figure 42: Second data set. Red graph describes the range of the measured angles. Blue graph shows the mean absolute deviation.

12.7 Angle of Attack test B, T7

The system did not succeed to estimate the Angle of Attack continuously when placed horizontally. The angle was sometimes estimated correctly but included a high spread of erroneous estimations.

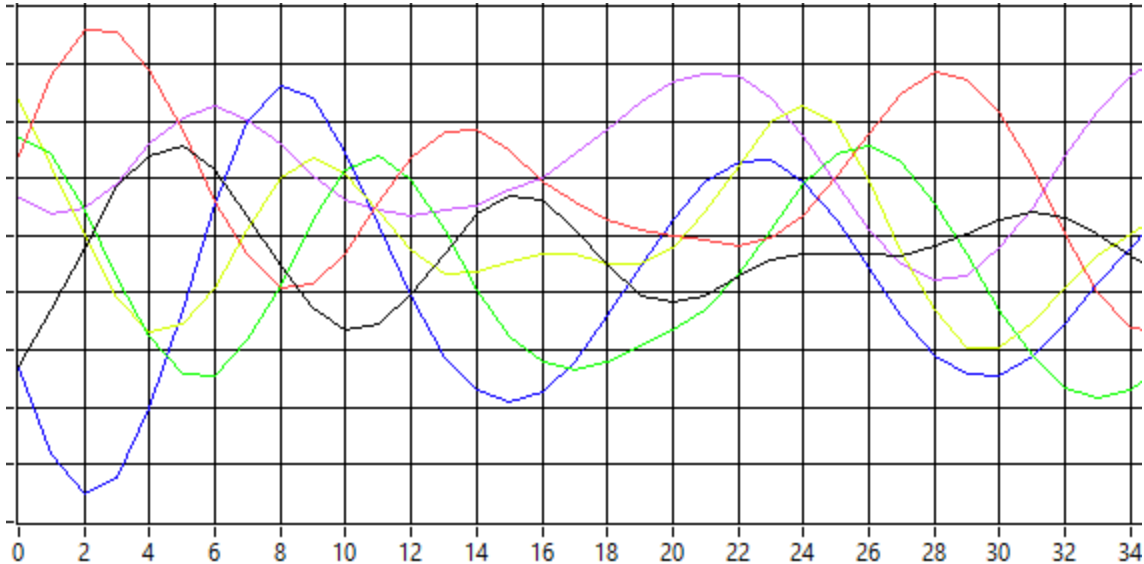


Figure 43: The graphs indicate the signals received by the 6 array elements after amplification and filtering. The phases of all channels except blue are shifted during the sequence causing the AoA estimation to fail.

12.8 Localization test, T8

The Test modem was localized and shown in the user interface at a distance of $1.05m$ from the Main modem. The estimated position was very responsive to the manual adjustments of the Main modem to the test rig. The position of the Test modem appeared to rotate around origin in figure 44 as response to manual adjustments of the test rig.

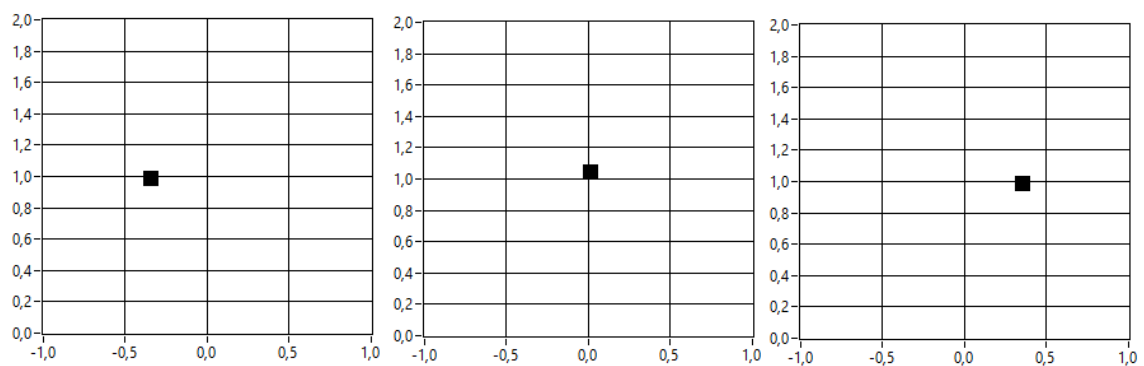


Figure 44: Localization performed in pool. Main modem is placed in the origin and attempts to locate the Test modem shown as a black dot. Results were obtained after filtering by EKF. Localization seemed smooth and responsive when rotating the Main modem and hence simulating that the Test modem rotates around the Test modem.

12.9 Planar wave propagation test, T9

The wave is received by the element pairs from first to last in the following order : (2,3),(1,4) and (0,5). Within each pair, the signal is received approximately at the same time. The outer elements are the last to receive the signal.

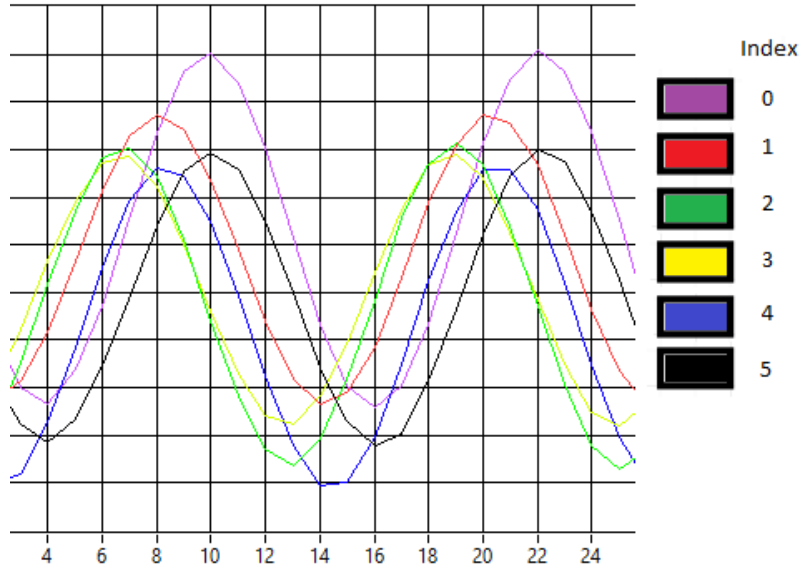


Figure 45: TDoA due to non planar propagation in terrestrial environment. Purple and black show the signal received by the outer elements and has the greatest phase shift. Green and yellow shows the signal received by the inner elements. Measurements was taken at a distance of 1m between test and Main modem.

12.10 Electronics and other results

The PSU, channel board and mother board were tested separately.

12.10.1 PSU testing

During design phase, the PSU was tested for noise level. The voltage between ground and $\pm 5v$ was measured. The electronics was routed on a breadboard with short jumper cables. The $\pm 100v$ DC/DC converted is active with pi-filter connected during measurement.

Table 5: Voltage measurements breadboard

Measurement	1	2	3
Gnd, +5v	5.7mVp-p	8.6mVp-p	5.6mVp-p
-5v-Gnd	5.9mVp-p	5.1mVp-p	6.0mVp-p

During final testing of PSU, the variable voltage range was measured for the high and low side supplies. Both supplies was able to output a voltage between $\pm 50 - 120V$ depending on the potentiometer input.

12.10.2 Channel board testing

The following parameters was included in the testing of the channel board. for current leakage, output, T/R switch and Filter performance.

12.10.3 No load current

The current draw of the channel board without load was measured to evaluate the current leak of having the P and N channel MOSFETS gates commonly controlled. The gate drivers was controlled by a PWM of 40kHz. A lab power supply was connected to the channel boards high voltage input. The high voltage supply voltage was varied between $\pm 16 - 32v$.

Table 6: Voltage measurements breadboard

Open Circuit voltage	$\pm 12v$	± 16	$\pm 20v$	± 24	± 28	± 32
Current	0.4mA	0.5mA	0.5mA	0.6mA	0.6mA	0.7mA

12.10.4 T/R switch

The T/R switch was tested with a sinus 5v peak amplitude at 40kHz. The voltage clip was triggered at 500mV.



Figure 46: Voltage clipping of a high voltage 40kHz signal due to the T/R switch. Voltage is limited to $\pm 1v$ and protects the sensitive amplifier stage.

12.10.5 Channel board Input

The antenna input of the channel board was connected to a function generator configured to generate a sinusoid at 100 kHz with 5mV peak amplitude. The channel board was configured to have a cutoff frequency of 140 kHz, PSU was never loaded during the tests. The following 3 images show the filter output during the following conditions.

1. PSU inactive, no input gain.
2. PSU active, no input gain.
3. PSU active, input gain of 16V/V.

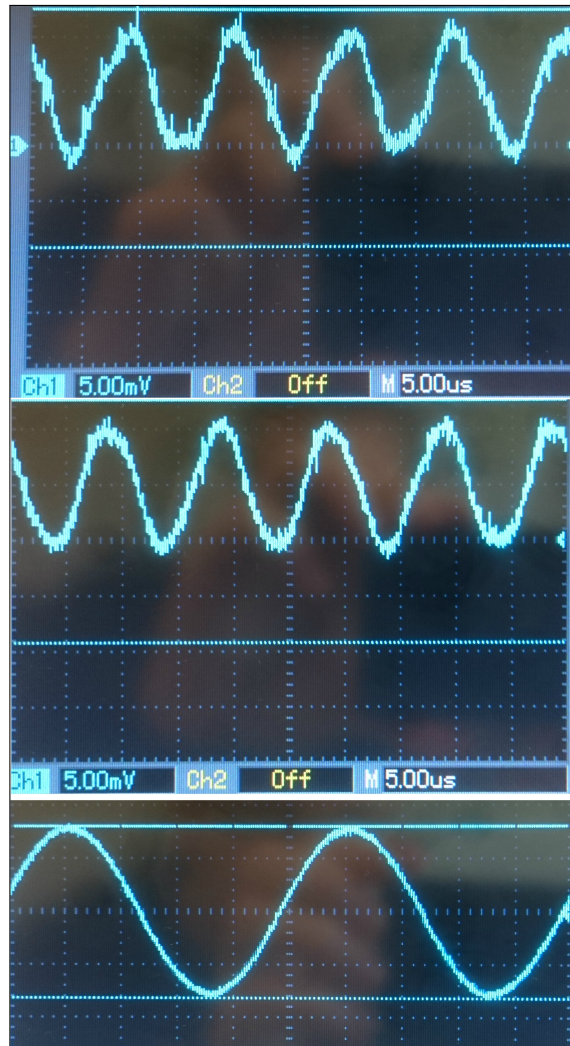


Figure 47: Filtering of signal through channel board.

High frequency noise is removed. Following images are shown in the figure from top to bottom,

- (1) PSU inactive, no input gain
- (2) PSU active, no input gain
- (3) PSU inactive, input gain of 16v/v

12.10.6 Channel board input filter

The channel board input filter was tested based on acoustic transmission generated by a transmitter. An oscilloscope was used to measure the received signal before and after filtering. Harmonics was observed before filtering with a cutoff at 70 kHz but was not observed after the filter.

12.10.7 Hardware in the loop RMS detector test

The RMS detector on FPGA was tested. The sensor was removed and stimuli was added to simulate received signals during the receiving slot. During the start of this slot a propagation delay was simulated by delaying the stimuli accordingly. After the delay, stimuli was added by transmitting on the receiving channel which is treated as a received signal. The RMS detector triggers with a difference ± 100 ticks at $40MHz$ which corresponds to an range measurement offset of $0.1295m$ at $c = 1480$.

13 Requirements verification

All hardware requirements **H1 - H5** were met. All performance requirements **P1 - P4** were met except part of **P3** which specifies a transmission distance of 20m. The system requirement **S1** - “simultaneous localization and communication” requires additional sensors, integration and testing to be fully verified.

13.1 System requirements verification

S1 could not be verified during testing. In order to verify the requirement, velocity sensors are needed for testing of the main modem. Furthermore, the model for localization has to be extended and integrated before complete system verification can done.

13.2 Hardware requirements verification

H1 was proven by **T2** (beamforming transmission) and **T3** (Beamforming reception test).

H2 was proven by **T6** (Angle of Attack Test A).

H3 was considered proven and by the result from “PSU testing” together with the reasoning about configurable frequency in the discussion section.

H4 was proven by **T1** (Phase controllability test).

H5 was proven by the result presented in section [12.10](#).

13.3 Performance requirements verification

P1 was proven as the beam was successfully steered 30 degrees in the **T3** (beamforming transmission test).

P2 has partly been met. Test **T4** (Communication test A) and **T5** (Communication test B) verifies communication of the desired data rate. **T2** and **T3** demonstrated that the beamformer is working, however, directed communication has not been tested.

P3 Has been met, the system can estimate the bearing angle for a node with less than 5 degree accuracy, the performance was tested in **T6** (Angle of Attack test A).

P4 has been met as the system can estimate the distance to a node with an error of around 5 cm. Verification was done by test **T8** (Localization test).

14 Discussion

All measurements which includes manual test rig adjustments have a degree of error due to interaction between the tester and test rig. The angular precision of test rig was considered in section 11.1, however, the limitation can only partly explain the results observed in the **T7** (Angle of Attack test B) where some of the measured angles differed from the expected angle significantly more than others. The results might be explained by environmental factors such as wind, water splashes or other errors during testing. Another limitation in the measurements is the angular resolution. During small changes between subsequent measurements this is of little importance, however, during fast changes in data it is desired to increase the angular resolution.

Test **T3** (Beamforming transmission test) shows that the transducer can produce a distinct gain pattern and that the main lobe can be steered. The observation fits the models of beam steering described by Sherman et al. [26]. The shape and strength of the beam pattern changes significantly with the angle. The expected second pair of side lobes can not be found, this is most likely due to the limited angular resolution as the difference between subsequent samples becomes high. An increased resolution would reduce the difference between samples and provide a better understanding of the actual beam pattern. For all tests, more measurement sets with higher angular resolution are preferable. Additionally, measurement errors are of more significance when measuring small values such as the intensity around the side lobes. The beam pattern can be affected by the directivity of the transducers, this could decrease the strength of the steered beam with respect to the angle. Furthermore the strength is also reduced by the steering angle as described in the literature due to interference. These two phenomena contribute to a total gain loss dependant on the steering angle, the proportions are currently not known or estimated.

The beamforming reception results are significant and clearly indicate a spatial filtering. The rapid gain decrease to a minimum around 20 degrees can not be explained by the directed elements and clearly proves the beamforming gain. The offset compensated results shows a peak around 0 degrees as expected. One or two pair of side lobes can be seen in the results, however it is hard to make further conclusions based of obtained measurements.

Angle of attack test proved to work depending on environment, in vertical configuration the test provided significant results while it failed in horizontal configuration. The results can be explained by that the signal received in horizontal mode include not only first arrivals, but also multipath propagation of the transmitted signal. The range of the measured values varied between 0.5 to 5 degrees, the mean absolute deviation was quite constant and was improved between the first and the second test. The measured range and mean absolute deviation seem random and it is hard to see any similarities between the sets. The measured values in the sets both follow the actual angle, the deviations from the actual value of the two sets seems not to be related to a significant degree. This can be explained by measurement errors and environmental conditions. The model for AoA estimation seem to be feasible as the data follows expected results

Test **T4** (Communication test A) and **T5** (Communication test B) demonstrated that the integrated communication and localization modem was capable of transmitting data using the chosen protocols. The performance were however sensitive for fluctuations in the environment and testing was limited to shorter distances only. The results confirmed the problems of multipath. The echoes generated inside the pool were significant to the degree that it was hard to distinguish signal from echo. The literature describes shallow water as the hardest environment to work with [42] and a pool should be even harder. From the result it is evident that a pool can be considered a poor choice of environment for testing since it doesn't represent the actual properties of an ocean or lake.

The Communication tests demonstrates how the acoustic channel distorts the phase of the transmitted signal, which is most likely the main cause of the limited performance of the communication. Even at the short distances of the performed tests a couple of periods was required of the carrier wave for the phase to stabilize fully. The phase distortion is probably a result several environmental and technological factors. Time-varying multipath and phase instabilities imposed by the

medium are probably the main source of the distortion. The mechanical properties of the piezo elements could also have a significant impact on the signal. Other sources of distortions could be the electrical filters of the Channel boards or the implemented signal processing software.

The requirements stated that the operating frequency of the system should be variable. The frequency is determined by FPGA hardware and ADC's, by the electronics filter and drivers as well as the transducer's frequency response. The system was initially designed for a carrier frequency of 100kHz which was chosen as the center frequency of the elements designed together with Deepvision AB, however in order to obtain transducers within the time frame of the project, the system was configured to work at 40kHz without redesigning the electronics. The cut-off frequency of electrical filters used in the Channel boards is configurable up to 150 kHz which determines the upper limit of the variable frequency of the system. The intention behind the requirement was to allow the system to work with various number of transducers.

15 Conclusion

A system for acoustic communication and localization testing was developed. The system proved to be able to localize and communicate with an acoustic source. The communication and the localization was dependant on the environment and multipath propagation shown to produce erroneous localization and communication. Results were presented describing how the environment can affect the functionality of the communication and localization system.

Problem 1. A transducer was designed and manufactured based on models for acoustic propagation models and general beamforming. The adopted embedded hardware platform and the developed electronics was shown to be usable for beam forming, localization and communication.

Problem 2. DPSK was selected and proved to work for communication at short range using with a data rate of the requirements. PSK was by electronics and embedded design simple to modulate. The single carrier frequency protocol also provided a reduction in complexity as the model for beam forming depends on frequency. The data link layer considerations was limited to medium access.

Problem 3. Localization can be integrated in the communication by extending a transmitted package with a localization tone as described in the method. A localization tone of 10 periods was used for phase estimation, the overhead was estimated to 0,7%. The results show that AoA can be estimated based on phase comparison between received signals.

Problem 4. Localization was implemented for static nodes based. The probabilistic model EKF was used to consider the probability of erroneous measurements assumption of no movement. The results indicated that the method can be used to reduce noise in the localization however a quantitative analysis is required to prove the validity of the results. An approach to extend EKF to model the velocity of the main- and test modem was proposed.

problem 5. Beamforming was modeled and successfully tested based on a desired steering angle. Steering an acoustic beam towards a localized node was not tested, an approach was described in the method.

The testing performed has considered static nodes and the different parts has been individually tested. The hypothesis can not be proven until the formulated problems have been answered and further testing has been performed on the integrated system for mobile nodes.

16 Future work

In order to complete the research question, more work needs to be done on integration of localization and communication. Synchronization was not considered in our work and well known methods needs to be adopted. More detailed tests needs to be made on beamforming based a transducer with higher precision and efficiency. Communication and beamforming have been tested separately and both have proven to work. In theory the two should operate well together but integration and further testing are needed to fully verify functionality.

In order to increase the performance of the communication and account for the ISI caused by time-varying multipath and phase instabilities, several approaches can be considered. M. Stojanovic and others [43] have demonstrated that decision feedback equalizer is a feasible solution for power efficient communications over both shallow- and deep water channels. The method tackles multipath by coherently combining multiple arrivals. As the underwater acoustic modem will be used for moving robots, the effects of doppler has to be modeled, F. Qu and his colleagues provides an overview of current methods [44]. Much more work needs to be done on multipath modeling for usage for communication in shallow water, F. De Rango describes his method in his work [45]. Communication between complete arrays should be tested and evaluated for multipath rejection. For better performance in multipath environment, cross correlation can work better. The algorithm can be used to find the shift between the signals which minimize the difference rather than work with absolute phases.

Models for localization of mobile nodes was not implemented. In probabilistic robotics [11] Mr.Thrun et al. propose an algorithm for simultaneous localization and mapping based on range and bearing measurements for static landmarks. The algorithms can be extended to track moving objects velocity can be estimated by doppler and phase shift or by communicating odometry measurements in a common reference frame.

The thesis is a first step to develop acoustic modem with localization for underwater robots. The followings tasks are required to continue the work: Continue testing on the developed modem as well as develop more robust method for communication and localization for general transducer constellations. Develop system specifications and system design for an integrated localization and communication system for usage in real application. Investigate a transducer constellation and model for beam forming usable in real applications, the test platform proposed by this thesis can be used throughout the testing and model verification. The transducer model should move the work to 3D applications. Investigate an embedded hardware system design, adapt and integrate the daughter board, motherboard, PSU, FPGA/Data acquisition platform and PC for a robot application. Customize an embedded hardware platform for the proposed design. Set up a good testing environment and port the developed software and FPGA blocks to the developed embedded platform. In order to shorten the development process, use 2 main modems instead of using of testing modems.

17 Acknowledgement

We would like to express our gratitude towards Andrey and Martin which supervised us through the project by good engagement and valuable remarks on the work. We would also like thank Mikael which proposed the thesis and provided valuable input during result analysis. A Big thanks to Deepvision for the comments on transducer and electronics design. Finally we would like to thank our loved ones which have supported us throughout the thesis work.

References

- [1] european commission community research and development information service. (2016) Swarms. [Online]. Available: http://cordis.europa.eu/project/rcn/197524_en.html
- [2] M. Stojanovic, "Recent advances in high-speed underwater acoustic communications," *Oceanic Engineering, IEEE Journal of*, vol. 21, no. 2, pp. 125–136, 1996.
- [3] R. G. Lyons, *Understanding Digital Signal Processing*, 1st ed. Boston, MA, USA: Addison-Wesley Longman Publishing Co., Inc., 1996.
- [4] J. G. Proakis, E. M. Sozer, J. A. Rice, and M. Stojanovic, "Shallow water acoustic networks," *Communications Magazine, IEEE*, vol. 39, no. 11, pp. 114–119, 2001.
- [5] M. Stojanovic, J. Catipovic, and J. G. Proakis, *Acoustic Signal Processing for Ocean Exploration*. Dordrecht: Springer Netherlands, 1993, ch. Coherent Communications over Long Range Underwater Acoustic Telemetry Channels, pp. 607–612. [Online]. Available: http://dx.doi.org/10.1007/978-94-011-1604-6_57
- [6] J. Partan, J. Kurose, and B. N. Levine, "A survey of practical issues in underwater networks," *ACM SIGMOBILE Mobile Computing and Communications Review*, vol. 11, no. 4, pp. 23–33, 2007.
- [7] M. Chitre, S. Shahabudeen, L. Freitag, and M. Stojanovic, "Recent advances in underwater acoustic communications x00026; networking," in *OCEANS 2008*, Sept 2008, pp. 1–10.
- [8] I. F. Akyildiz, D. Pompili, and T. Melodia, "Underwater acoustic sensor networks: research challenges," *Ad Hoc Networks*, vol. 3, no. 3, pp. 257 – 279, 2005. [Online]. Available: <http://www.sciencedirect.com/science/article/pii/S1570870505000168>
- [9] W. van Kleunen, K. Blom, N. Meratnia, A. Kokkeler, P. Havinga, and G. Smit, "Underwater localization by combining time-of-flight and direction-of-arrival," in *OCEANS 2014 - TAIPEI*, April 2014, pp. 1–6.
- [10] N. Y. Ko, T. G. Kim, and Y. S. Moon, "Particle filter approach for localization of an underwater robot using time difference of arrival," in *OCEANS, 2012 - Yeosu*, May 2012, pp. 1–7.
- [11] S. Thrun, W. Burgard, and D. Fox, *Probabilistic Robotics (Intelligent Robotics and Autonomous Agents)*. The MIT Press, 2005.
- [12] B. Van Veen and K. Buckley, "Beamforming: a versatile approach to spatial filtering," *ASSP Magazine, IEEE*, vol. 5, no. 2, pp. 4–24, April 1988.
- [13] T. Haynes, "A Primer on Digital Beamforming."
- [14] S. Hossain, M. Islam, and S. Serikawa, "Adaptive beamforming algorithms for smart antenna systems," in *Control, Automation and Systems, 2008. ICCAS 2008. International Conference on*, Oct 2008, pp. 412–416.
- [15] G. Henderson, A. Tweedy, G. Howe, O. Hinton, and A. Adams, "Investigation of adaptive beamformer performance and experimental verification of applications in high data rate digital underwater communications," in *OCEANS '94. 'Oceans Engineering for Today's Technology and Tomorrow's Preservation.' Proceedings*, vol. 1, Sep 1994, pp. I/296–I/301 vol.1.
- [16] Evologics. (2016) Evologics underwater acoustic modem. [Online]. Available: https://www.evologics.de/en/products/USBL/s2cr_48_78_usbl.html
- [17] DSPComm. (2016) Dspcomm underwater acoustic modem. [Online]. Available: http://www.dspcomm.com/products_aquacomm.html
- [18] Tritech. (2016) Micron data modem underwater acoustic modem. [Online]. Available: <http://www.tritech.co.uk/product/micron-data-modem>

- [19] WHOI. (2016) Whoi micro modem. [Online]. Available: <http://acomms.whoi.edu/micro-modem/>
- [20] Benthos. (2016) Benthos dat. [Online]. Available: http://teledynebenthos.com/product/positioning_systems/benthos-dat
- [21] Linkquest. (2016) Linkquest uwm2000. [Online]. Available: <http://www.link-quest.com/html/uwm2000.htm>
- [22] J. Wills, W. Ye, and J. Heidemann, "Low-power acoustic modem for dense underwater sensor networks," in *Proceedings of the 1st ACM International Workshop on Underwater Networks*, ser. WUWNet '06. New York, NY, USA: ACM, 2006, pp. 79–85. [Online]. Available: <http://doi.acm.org/10.1145/1161039.1161055>
- [23] I. Vasilescu, C. Detweiler, and D. Rus, "Aquanodes: an underwater sensor network," in *Proceedings of the Second Workshop on Underwater Networks, WUWNET 2007, Montréal, Québec, Canada, September 14, 2007*, 2007, pp. 85–88. [Online]. Available: <http://doi.acm.org/10.1145/1287812.1287830>
- [24] J. A. Neasham, G. Goodfellow, and R. Sharphouse, "Development of the x201c;seatrac x201d; miniature acoustic modem and usbl positioning units for subsea robotics and diver applications," in *OCEANS 2015 - Genova*, May 2015, pp. 1–8.
- [25] E. M. Sözer and M. Stojanovic, "Reconfigurable acoustic modem for underwater sensor networks," in *Proceedings of the 1st ACM International Workshop on Underwater Networks*, ser. WUWNet '06. New York, NY, USA: ACM, 2006, pp. 101–104. [Online]. Available: <http://doi.acm.org/10.1145/1161039.1161060>
- [26] C. H. Sherman and J. L. Butler, *Transducers and Arrays for Underwater Sound*. Springer Publishing Company, Incorporated, 2007.
- [27] A. D. Waite, "Sonar for practising engineers."
- [28] X. Lurton, *An introduction to underwater acoustics : principles and applications*. London ; New York : Springer, 2002, includes bibliographical references and index.
- [29] *Waterproof type ultrasonic sensor, A-14P20 datasheet*, EKULIT.
- [30] *USB-7845R, R Series Multifunction RIO With Kintex-7 70T FPGA*, National Instruments, 2014.
- [31] *Quad Comparator, LTC1564 datasheet*, Fairchild, 2012, rev. 1.0.5.
- [32] *Series Voltage Regulators, LM78XX datasheet*, Texas Instruments, 04 2013.
- [33] *Series 3-Terminal Negative Regulators, LM79XX datasheet*, Texas Instruments, 04 2013.
- [34] *DC/DC-Converter, R05-100B datasheet*, RECOM, 2015, rEV: 0/2015.
- [35] *N- and P-Channel Enhancement-Mode MOSFET Pair, TC6320 datasheet*, Supertex inc., 06 2016.
- [36] *High Speed, Dual MOSFET Driver, MD1211 datasheet*, Supertex inc., 02 2012.
- [37] *Antialiasing Filter and 4-Bit P.G.A., LTC1564 datasheet*, Linear Technology.
- [38] *High Voltage Protection T/R Switch, MD0100 datasheet*, Supertex inc., 7 2014.
- [39] *NI myRIO-1900, Embedded Student Design Device*, National Instruments.
- [40] *Single Rail-to-Rail Ultralow 1.9nV/Hz Noise, Low Power Op, 100MHz Amps, LT6202 datasheet*, Linear Technology.

- [41] I. F. Akyildiz, D. Pompili, and T. Melodia, “Challenges for efficient communication in under-water acoustic sensor networks,” *ACM Sigbed Review*, vol. 1, no. 2, pp. 3–8, 2004.
- [42] D. B. Kilfoyle and A. B. Baggeroer, “The state of the art in underwater acoustic telemetry,” *Oceanic Engineering, IEEE Journal of*, vol. 25, no. 1, pp. 4–27, 2000.
- [43] M. Stojanovic, J. Catipovic, and J. G. Proakis, “Adaptive multichannel combining and equalization for underwater acoustic communications,” *The Journal of the Acoustical Society of America*, vol. 94, no. 3, 1993.
- [44] F. Qu, Z. Wang, L. Yang, and Z. Wu, “A journey toward modeling and resolving doppler in underwater acoustic communications,” *IEEE Communications Magazine*, vol. 54, no. 2, pp. 49–55, February 2016.
- [45] F. D. Rango, F. Veltri, and P. Fazio, “A multipath fading channel model for underwater shallow acoustic communications,” in *2012 IEEE International Conference on Communications (ICC)*, June 2012, pp. 3811–3815.